

PROCESS MODELING OF FORWARD OSMOSIS AND PRESSURE
RETARDED OSMOSIS INTEGRATION WITH SEAWATER REVERSE
OSMOSIS

by

Zachary M. Binger

Copyright © Zachary M. Binger 2020

A Thesis Submitted to the Faculty of the

DEPARTMENT OF CHEMICAL AND ENVIRONMENTAL ENGINEERING

In Partial Fulfillment of the Requirements

For the Degree of

MASTER OF SCIENCE

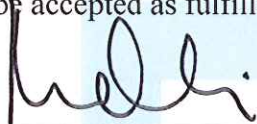
In the Graduate College

THE UNIVERSITY OF ARIZONA

2020

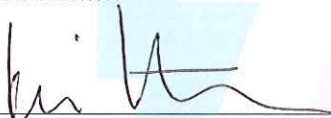
THE UNIVERSITY OF ARIZONA
GRADUATE COLLEGE

As members of the Master's Committee, we certify that we have read the thesis prepared by Zachary Binger, titled PROCESS MODELING OF FORWARD OSMOSIS AND PRESSURE RETARDED OSMOSIS INTEGRATION WITH SEAWATER REVERSE OSMOSIS and recommend that it be accepted as fulfilling the dissertation requirement for the Master's Degree.



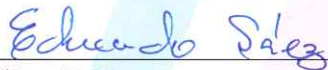
Andrea Achilli

Date: 1/14/2020



Kerri Hickenbottom

Date: 1/14/2020

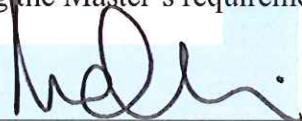


Avelino E. Saez

Date: 1/14/2020

Final approval and acceptance of this thesis is contingent upon the candidate's submission of the final copies of the thesis to the Graduate College.

I hereby certify that I have read this thesis prepared under my direction and recommend that it be accepted as fulfilling the Master's requirement.



Andrea Achilli
Master's Thesis Committee Chair
Chemical & Environmental Engineering

Date: 1/14/2020

ARIZONA

Table of Contents

List of Figures and Tables	4
Abstract	6
1. Introduction.....	7
1.1. Forward Osmosis (FO)	7
1.1.1. Forward Osmosis Modeling and Theoretical investigations	10
1.2. Pressure Retarded Osmosis (PRO)	13
1.2.1. Pressure Retarded Osmosis Modeling and Theoretical investigations	14
1.3. Objective of Study	18
2. Materials and methods	19
2.1. FO and PRO process configuration	21
2.2. Module geometry	27
2.3. Module discretization.....	29
2.3.1. Iteration Scheme	29
2.3.2. Governing Equations	31
3. Results.....	35
3.1. Plate and Frame vs Spiral Wound.....	35
3.2. Configuration sensitivity to changes in operating conditions.....	37
4. Conclusions.....	47

LIST OF FIGURES AND TABLES

Figure 1. Illustration of spiral-wound and hollow fiber membranes.....	10
Figure 2. Representative plot of the osmotic pressure difference of a seawater draw stream and river water feed stream as a function of volume permeated.....	16
Figure 3. Illustration of the inverse relationship between power density and specific energy recovery.....	17
Figure 4. Hypothetical water cycle with FO-RO process.....	19
Figure 5. Hypothetical water cycle with RO-PRO process.....	20
Figure 6. Simplified illustration showing the input and output of the process streams for the recirculation and recharge configurations.....	22
Figure 7. Illustration of the concentrations of both process streams for a single-stage non-recharge without recirculation and multi-stage recharge configurations for a forward osmosis process as a function of position along the length of the process.....	23
Figure 8. Illustration of the concentrations of both process streams for a single-stage non-recharge and multi-stage recharge configurations for a pressure retarded osmosis process as a function of position along the length of the process.....	24
Figure 9. Model logic flow chart for FO and PRO.....	25
Figure 10. Illustration of the proposed configuration for an FO unit process.....	26
Figure 11. Illustration of the proposed configuration for a PRO unit process.....	27
Figure 12. Illustration of a realistic flow path in a spiral-wound membrane and simplified flow path for modeling purposes.....	28
Figure 13. Iteration scheme of a plate-and-frame model. The streams interactions can be either co-current or counter-current and are updated sequentially.....	30
Figure 14. Iteration scheme and arrangement of a “cross-flow” model.....	30
Figure 15. Membrane arrangement and concentration profile for FO and PRO processes.....	32
Figure 16. Contour plot illustrating the effect of flow conditions on the specific energy recovery for a single plate-and-frame module and a single spiral-wound module.....	36

Figure 17. Contour plots illustrating the feed utilization, specific energy consumption, RO influent concentration, and average flux for the FO process without recharge or recirculation.....38

Figure 18. Contour plots illustrating the feed utilization, specific energy consumption, RO influent concentration, and average flux for the FO process without recharge with the use of recirculation..... 40

Figure 19. Contour plots illustrating the feed utilization, specific energy consumption, RO influent concentration, and average flux the for the FO process with recharge.....42

Figure 20. Contour plot illustrating the effect of flow conditions on the specific energy recovery of a PRO process arranged in a series configuration without recharge and with recharge.....43

Figure 21. Contour plots illustrating the effect of membrane characteristics on the specific energy recovery of a PRO process a series configuration without recharge and with recharge.....45

Figure 22. Contour plots illustrating the effect of membrane characteristics on the power density of a PRO process a series configuration without recharge and with recharge.....46

Table 1. Membrane parameters used in modeling.....28

Abstract

Osmotically driven membrane processes, like forward osmosis and pressure retarded osmosis, may hold key advantages when integrated with reverse osmosis for seawater desalination. The spiral-wound membrane platform in which these processes are applied has inherent disadvantages that need to be explored. Maintaining proper operating pressure in both of the fluid channels of a spiral-wound membrane requires the feed and draw streams to be operated at different flow rates, often as drastic as a 1:10 ratio. This affects the thermodynamic equilibrium of the system and drastically affects potential water and energy recovery.

In this work, a model was created to rigorously represent spiral-wound membranes to increase modeling accuracy. A process configuration that features periodic recharging of the stream inside of the envelope is proposed to mitigate the effects of the flow rate difference. The model is used to compare the multi-stage design to single-stage configurations for both forward osmosis and pressure retarded osmosis by testing various feed and draw flow rate ratios, between 1:10 to 1:1, operated by each process as well as important membrane characteristics such as channel height and water and salt permeability.

The multi-stage design shows an increase in wastewater utilization from 62.6% to 90% when compared to the single-stage designs for forward osmosis. Additionally, the multi-stage configuration increases the pressure retarded osmosis specific energy recovery from 0.13 kWh/m³ to 0.55 kWh/m³. However, the increased effectiveness of these multi-staged designs comes with a reduction in average water flux and power density, which leads to the requirement of more membrane area and capital investment for potential system implementation.

1. Introduction

Due to the increasing global population and water demand, securing reliable and sustainable water sources will remain a major challenge for scientists and engineers for the foreseeable future. Seawater desalination through reverse osmosis (RO) is one technology that will continue to play a critical role in securing a diverse water source portfolio [1].

However, the potential environmental impact of seawater RO (SWRO) requires thoughtful engineering designs to ensure desalination waste streams such as high concentration brine streams don't negatively impact oceanic ecosystems [2]. Some governments have already made steps to making this a priority. Currently in California, to mitigate environmental impacts, the brine stream of a desalination process must be diluted to levels that are essentially equivalent to the ocean concentration [3]. This requires a low salinity water source to act as a diluent and one readily available choice is treated wastewater.

Although the use of treated wastewater to dilute SWRO concentrate is central to solving the RO concentrate disposal dilemma, it assumes there is a plentiful and disposable supply of treated wastewater. However, because of increased conservation, wastewater flows have declined; and more importantly, as more wastewater is being reclaimed for reuse purposes, less treated wastewater is being discharged to the ocean. For this reason, it is imperative to make greater beneficial use of the treated wastewater.

1.1. Forward Osmosis (FO)

Forward Osmosis can be integrated into the front-end of an SWRO process to create a hybrid FO-RO process [4, 5]. In FO, the flow of water across the semi-permeable membrane occurs due to the osmotic pressure difference between the two sides of the membrane. This process is operated with no energy cost for transmembrane flow except that which is required to circulate

solutions in the system. The goal of the FO process in an FO-RO system is to dilute the incoming seawater stream. By doing so, the RO process requires less pressure to overcome the osmotic pressure of the influent stream and will require less energy to produce the same quantity of permeate as a non-diluted influent stream. Overall, the reuse of wastewater is beneficial in an FO-RO system for energy reduction of the RO process, but also for lowering the RO brine discharge concentration. By using the FO process's permeate flow rate to decrease the RO influent concentration, the resulting RO brine concentration can be controlled for an RO process operating at a fixed recovery rate. The advantages of the FO-RO process include:

- Lower energy usage for seawater reverse osmosis desalination through brine dilution [4, 5]
- Reduction in RO fouling and scaling [6]
- Multi-barrier treatment of wastewater and high rejection [5, 7]
- Beneficial reuse of wastewater for achieving RO brine discharge [8]

Results from pilot-scale experiments have shown that, although the membrane can heavily foul with suspended solids, flux decline is minimal and chemical cleaning efficiently restores flux to its initial level [7]. It has also been shown that despite the high loading of dissolved and suspended materials, FO was capable of maintaining acceptable water flux and experienced mostly reversible fouling [8]. Similarly, studies have shown that FO-RO has a much lower scaling propensity and can be operated for a much longer operation period at higher water recovery without cleaning process compared to standalone RO [6]. There is ample evidence that FO can be implemented to utilize feed streams of variable qualities with minimal decline in performance [5, 7].

Pilot-scale experiments have also shown that more than 97 percent ammonia and nitrate can be effectively removed and with the two barriers (FO and RO membranes) [9]. The

concentration of many constituents commonly to be treated by an FO-RO system has been shown to be reduced to levels lower than EPA primary drinking water standards, highlighting the ability for the system to treat impaired water for direct potable reuse [9, 10].

The two most common platforms to perform forward osmosis are spiral-wound membrane (SWM) modules (Figure 1a) and hollow fiber (HF) modules (Figure 1b) [11]. SWMs consist of a large flat sheet of membrane, folded onto itself to form an envelope, and wrapped around a central tube. That is, one stream flows outside of the envelope in the direction of the length of the module (feed side in FO, draw side in PRO), and the other flows inside the envelope in the direction of the long dimension of the membrane (draw side in FO, feed side in PRO). Often, a single module can be comprised of multiple flat sheets, or leaves, to maximize the membrane area available in the footprint of a single module. In between the layers of the membrane, spacers are added to provide structural integrity to prevent the membrane from deforming under pressure as well as promote turbulence for increased mass transfer. Similarly, HF modules are comprised of many tube-like fibers arranged in a bundle inside a protective shell. In HF modules, one process stream is distributed and channeled inside the hollow fiber tubes while the other process stream is sent of the space between the hollow fibers and the protective shell. Both of these designs are advantageous for packing a large amount of membrane area into a small footprint and creates a modular design for easy implementation and switching out of modules during maintenance.

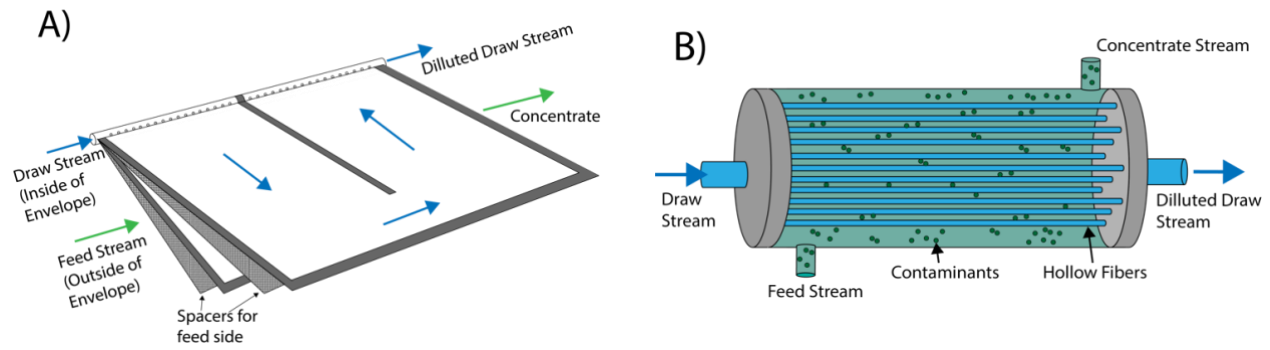


Figure 1. A) Illustration of spiral-wound membrane module showing how the two process streams are arranged as well as the inclusion of spacers and baffling. Illustration of spacers on the draw side were omitted for visual clarity of draw flow path and channel distinction but would be present in physical systems. B) Illustration of hollow fiber module showing the outer shell and the bundle of hollow fiber tubes present that reject contaminants and captures the permeate.

1.1.1. Forward Osmosis Modeling and Theoretical investigations

Several FO-RO numerical models have been created [6, 12-14]. Results of these modeling highlighted that implementing FO lowers the specific energy consumption (SEC) (kWh/m³) compared to a baseline SWRO [13], that FO-RO hybrid integration can be beneficial only if substantial energy and operating costs savings over standalone RO are obtained by adding the FO process to offset the increased capital and operational costs [13], that FO models are reasonably accurate at estimating water flux [6, 14] but they regularly underestimate the energy consumption for overcoming pressure losses, and that an average permeation flux of 30 LMH is a plausible threshold to guarantee FO economic stability [13].

An FO-RO model was used to perform a life cycle assessment of a water treatment system producing 100,000 m³/day, showed that compared to SWRO as a baseline, an FO-RO system has a higher capital cost but a significantly lower operations cost due to savings in energy

consumption and fouling control [15]. Another theoretical study found that based on the cost of energy and current cost of FO membranes (~\$12/m²), the osmotic dilution process is economically viable for a small treatment plant (~200 m³/day) to recover up to 60 percent of an impaired stream [9]. Beyond that recovery, the capital cost associated with installing additional osmotic dilution membrane capacity becomes greater than the money saved from reduced energy consumption of the SWRO process.

The study by Altaee et al. [12] found that the efficacy of FO implementation changes if an energy recovery device (ERD) is used. The results show that for a small SWRO facility without ERD, the specific energy consumption (SEC) of permeate production was between 5.22-6.97 kWh/m³. For the same operating conditions, the energy of an FO-RO system was between 4.32-5.80 kWh/m³, indicating that FO-RO system was more energy efficient. However, when a highly efficient ERD (80-95% efficiency) was employed the SEC reduced to 2.54- 2.84 kWh/m³ for the conventional RO unit, whereas for the FO-RO system it was between 2.53-2.95 kWh/m³. Using a high-efficiency ERD reduced the energy cost of the RO to a point where it became more competitive than FO-RO even at high feed salinities. The data in this study suggests that the FO process didn't significantly reduce the energy cost of the RO process compared to conventional RO. However, one distinct difference between the results for conventional RO and FO-RO systems, is that the increase in the energy cost of the RO process over multiple years of operation is much less rapid in the FO-RO system. These findings indicate that the addition of FO might be best utilized by small desalination plants without ERD systems and highlights the advantage of adding FO with feed waters that have a high potential for fouling.

In these FO-RO models and many other standalone FO models [6, 12, 14, 16-20], there is a shortcoming in the way the module is represented. These models represent the FO modules as

plate and frame modules operating in co-current or counter-current modes. Modeling that accounts for specific operational aspects of spiral-wound modules, such as the cross-flow operation, is limited [21] and none of which have been applied to FO-RO models. The modeling by Gu et al. [21] was thorough in representing both plate-and-frame and spiral-wound modules. However, the discretization and declaration of multiple regions along the membrane, with their own unique contributions to the permeate flux, is complex and can be simplified.

Issues with modeling FO using a flat plate model go beyond the accurate representation of stream interaction, but spiral-wound modules present operational limitations inherent to their geometry and configuration that need to be considered by models. In a SWM the feed and draw stream channels each have a unique resistance that is dependent on their features such as the channel length, width, height, the baffling, and the spacer type used. These unique resistances will result in different pressure-flow relationships for each stream [10, 22, 23]. For example, the channel inside the envelope has a narrower channel width, typically has a much longer flow path than the channel outside of the envelope, and a baffle that requires the stream to flow around the bend (illustrated in Figure 1a). These characteristics mean that the stream inside the envelope will experience higher pressure drops than the channel outside of the envelope. This phenomenon has been shown to apply to hollow fiber membranes as well [24]. Because of these differences in the hydraulic resistance, it will not be possible to operate the FO module with equal draw and feed flow rates without reducing the driving force for water flux due to the resulting pressure imbalance.

In FO, and in any process that utilizes a thin film composite membrane comprised of a dense selective layer on top of a porous support, the dense layer of the membrane must always be facing the higher pressure side of the membrane to avoid delamination of the dense layer itself.

In FO, the dense layer faces the feed solution as it is the side that is less susceptible to fouling. Because of this, often the ratio between the streams inside and outside of the envelope is between 1:5 and 1:10 [10, 22] depending on the configuration of the module. The potential for delamination or module damage is further exacerbated as the percentage of feed stream utilization is increased [10]. As recovery increases so does the pressure at the inlet of the draw side, inside of the envelope, due to the increased flow rate downstream. This can be avoided by applying pressure on the feed side, however, it will increase the energy required by the FO process and may exceed the safe pressure operation of the module.

It has been suggested that to safely accommodate for feed recovery rates, an FO process must use lower initial draw stream flow rates and a higher number of FO elements [10]. In the same study it was found that for an FO desalination plant of fixed capacity, the initial draw stream flow rate and concentration correlate inversely and must be complemented with a higher draw stream concentration. This poses a challenge if seawater is used as the draw stream since it is a fixed concentration. To achieve enhanced feed recovery rates with a fixed concentration draw stream and a fixed target desalination capacity, simple arrangements of multiple elements in series may not be sufficient and further research on system configurations is necessary to improve the technology.

1.2. Pressure Retarded Osmosis (PRO)

Similar to the FO-RO system, pressure retarded osmosis (PRO) can be integrated on the back end of an RO process to create a hybrid RO-PRO system [25, 26]. The high concentration brine from the RO reject can be used to create a large osmotic pressure difference that PRO can use to recover energy. PRO recovers this energy by using this osmotic pressure difference to drive permeate across the membrane from the feed to draw side against a pressure gradient. In PRO

the draw stream is pressurized and the resulting diluted draw stream is then passed through an energy recovery device (ERD) that can be used to exchange pressure to the RO inlet stream [27, 28]. ERDs are commonly used in RO processes and the added flow rate due to the PRO permeate increases the amount of energy recovered. As a result, the chemical potential from the osmotic gradient is effectively converted into mechanical energy.

In addition to energy recovery, PRO also dilutes the RO brine stream prior to discharge due to the added permeate in the draw stream. The ideal operation of PRO would result in the brine stream being diluted below environmental discharge regulations[3]. However, achieving that level of dilution requires a system design that can extract the necessary amount of permeate, which proves difficult due to the diminishing driving force that occurs in a PRO process as the draw stream is diluted [29].

Pilot-scale and module-scale experiments of PRO are limited [25, 30, 31]. Results of module-scale PRO operation have shown power densities as high as 8 W/m², but due to energy consumption for pumping the feed and draw streams the effective net energy savings may even be negative. This highlights the struggle of scaling PRO to the module and process scale. Operation of PRO using spiral-wound modules will require careful consideration of membrane characteristics and module configuration to become viable.

1.2.1. Pressure Retarded Osmosis Modeling and Theoretical investigations

Multiple studies have looked at the thermodynamic and energy efficiency for RO-PRO systems [32-37]. Findings in modeling RO-PRO systems include:

- Operational conditions of RO are the dominant influence on RO-PRO effectiveness and a decrease in the RO process size significantly reduces the cost effectiveness of an RO-PRO system [32].

- Lower RO water recovery and higher ratio of the PRO feed flow rate to the combined PRO feed and draw flow rates improve the stand-alone feasibility of the hybrid system [33]
- Best operating conditions and specific energy are both functions of the initial feed and draw concentrations, and are independent of any properties of the module [38].
- For asymmetric membranes, the power density may be substantially reduced due to severe internal concentration polarization and, to a lesser degree, to reverse salt diffusion [36].

Of these studies of RO-PRO systems there are some key takeaways. Studies modeling the PRO process have found that the composition and quantity of the two streams available dictate a theoretical maximum for the amount of energy that can be recovered and the power density of a module [38, 39]. The highest extractable work in constant-pressure PRO with a seawater draw solution and river water feed solution is 0.75 kWh/m³ [38-40]. Constant pressure PRO is not able to extract all of the available energy of the process because the applied pressure will cause the driving force to terminate before all of the permeate is extracted from the feed stream [39].

PRO has the highest power density when the applied pressure on the draw stream is equal to half of the osmotic pressure difference of the feed and draw streams [36]. As PRO proceeds and water permeates the membrane the feed concentration will increase while the draw concentration decreases, causing the osmotic pressure difference to diminish [39]. In Figure 2, the black line represents the dynamic osmotic pressure difference plotted as a function of the volume of water permeated [39]. As the volume of permeate approaches the final total permeate volume (ΔV_f), the osmotic pressure difference approaches zero. The theoretical work extractable is equivalent to the area under the curve, however, for a constant-pressure PRO process all the theoretical work is not extractable due to frictional losses (red shaded region) and the unutilized energy (green shaded region). The practical work extractable by constant-pressure PRO is shown by the

blue region. The unutilized energy is a result of the fixed applied pressure causing early termination of the driving force. This is defined as the flux termination point, where the net driving force of the water permeation between the two sides of the membrane is zero[39]. As PRO proceeds, the water flux decreases, causing the membrane power density to diminish and eventually permeate extraction ceases, leaving a remaining quantity of energy unutilized. For example, a PRO process operating with a pressurized draw stream at the best setting for power density will at most recover a permeate volume equal to the original draw volume. This is because when the osmotic pressure difference reaches half of its original value, the osmotic pressure difference and the applied pressure will be equivalent.

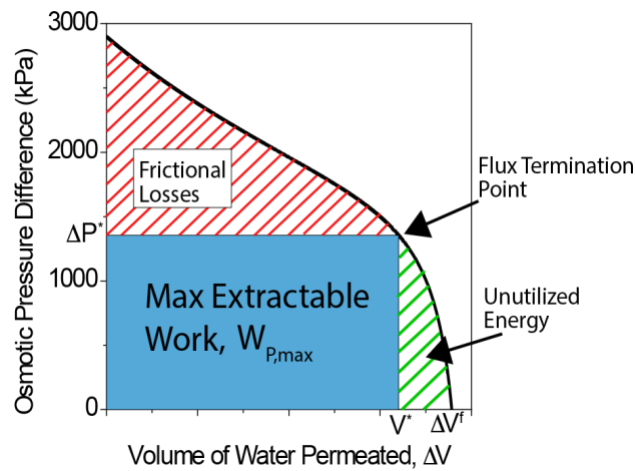


Figure 2. Representative plot of the osmotic pressure difference of a seawater draw stream with concentration of 35 g/L and river water feed stream with concentration 1 g/L as a function of volume permeated. As water permeates, the feed concentration increases while the draw concentration decreases resulting in $\Delta\pi$ decreasing to zero as ΔV increases towards the final total permeate volume ΔV_f . The blue colored area represents the maximum extractable work for a constant pressure PRO process. Adapted from Yip et al. [28].

It is evident that the objectives of maximizing power density and maximum energy extraction are not mutually attainable, illustrated in Figure 3. Figure 3 shows the inverse relationship between power density and energy recovery as a function of membrane area. A practical PRO system will need to balance the two objectives through optimizing operating parameters like applied hydraulic pressure and process termination point to maximize the effectiveness of implementing PRO to a hybrid RO-PRO system [39].

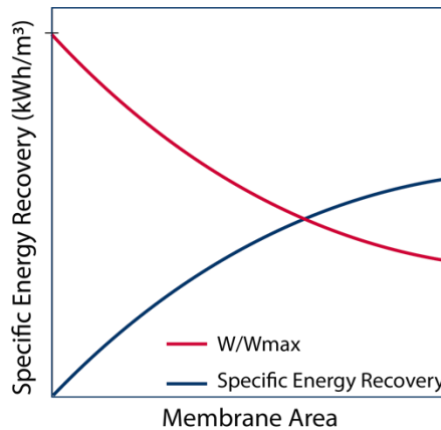


Figure 3. Magnitude and direction of J_w for FO, PRO, and RO with power density (W) plotted vs applied pressure, adapted from Achilli et al [31]. (Right) Illustration of the inverse relationship between power density and specific energy recovery. This figure shows that high power density and high energy recovery are not mutually attainable. Adapted from Ramon et al. [41].

Similar to FO-RO, a key shortcoming to RO-PRO models is that the current geometries used in PRO modeling do not reflect the spiral-wound modules used [26, 32, 36, 42]. This also goes beyond accurate representation of stream interaction, but similarly to FO, the feed and draw streams cannot be operated at similar flow rates. However, in PRO, the feed side is the channel inside the envelope, hence with the low flow rate potential, as it is the stream at lower pressure.

Even with very high recovery of the feed side, the draw side cannot be sufficiently diluted as the feed side is only a fraction of the draw side. As the amount of energy to be recovered in PRO directly dependent on the volume of permeate recovered, this also limits the amount of energy that can be recovered [39].

1.3.Objective of Study

The objective of this study is to create a modeling framework that can be used to quantify the impact of module geometry and process configuration on the permeate recovery and energy savings of FO-RO and RO-PRO systems. The process model created in this work expands on previous work by accounting for features such as module configuration (cross-flow orientation, baffling, maximum module flow rates) and stream recirculation to optimize a single treatment train to satisfy a user defined target for the utilization of wastewater and discharge concentration of RO brine. The model calculates the energy reduction for potable water production by integrating FO and PRO with SWRO. Considering the primary goals of utilizing FO-RO and RO-PRO are to reduce both energy and environmental footprint, a high utilization (> 90%) of wastewater was selected. This recovery target is implemented to minimize the amount of treated wastewater unutilized. Considering that the treatment of the wastewater has an associated energy cost it would be best practice to reduce the amount of this valuable stream being unutilized. This does impose a difficult requirement that demands many membranes in series, but the trade-off of the increased energy demand in FO and PRO to achieve this target is assumed to be a worthwhile exchange to reduce the waste of a valuable resource. Additionally, a maximum discharge concentration of 40 g/L was required to reflect currently established regulations[3].

The results of this study illustrate the impact that the ratio of flow rates inside and outside of the envelope have on water recovery and proposes a configuration that compensates for feed-draw imbalance to reach desired treated wastewater recovery.

2. Materials and methods

This study captures the operation of FO-RO and RO-PRO systems for seawater desalination in a steady-state balance of consumption and generation of SWRO permeate. It is assumed that RO is operated at 50% recovery and the resulting product water is used by a municipality and eventually be recycled back through a wastewater treatment plant. Figure 4 illustrates an ideal case where an FO-RO system would be implemented in a sustainable manner.

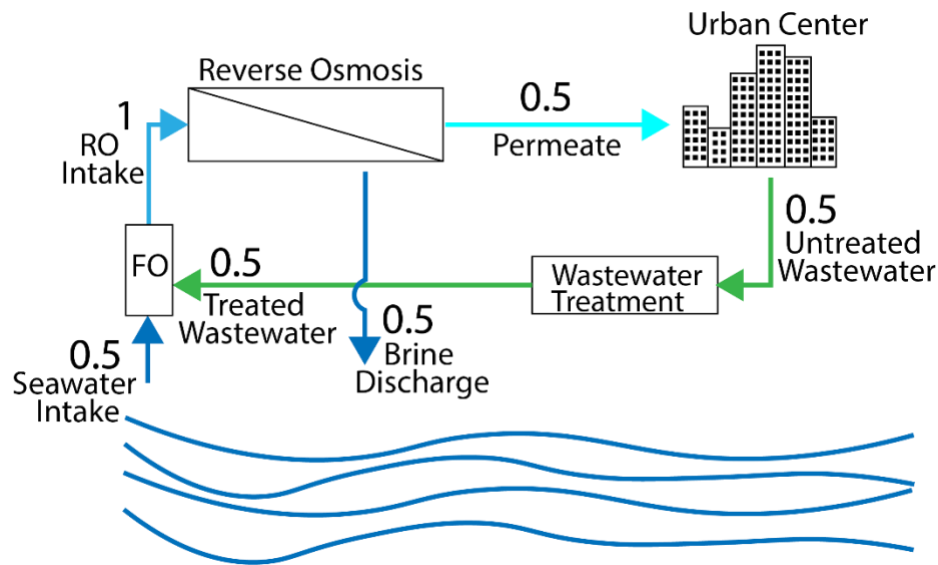


Figure 4. Hypothetical water cycle with FO-RO process. Values adjacent to the process lines represent the magnitude of flow rate through that particular segment of the process. In this scenario 0.5 parts seawater are combined with 0.5 parts wastewater to comprise the RO intake to be treated. The resulting permeate is then utilized by a municipality and recycled through a wastewater treatment plant before returning to be utilized as the feed stream for the FO process.

For every quantity of water processed by RO (assuming 50% recovery), equal amounts of permeate and brine will be produced. It is assumed in this type of application that the amount of wastewater available and returned to the system, in the form of treated wastewater to be used as the FO diluent, is also equal to the RO permeate. This creates a case where the intake and discharge to the ocean are of equal quantity and the characteristics of the discharge, mainly salt concentration, are closely matched to the background salt concentration to have minimal disturbance to the ocean ecosystem.

Similarly to FO, the study for PRO analyzes a balanced case where the seawater intake and brine discharge to the ocean are of equal quantity, shown in Figure 5. For every 1 part of seawater utilized by reverse osmosis, half will become potable water used by an urban center while the other half becomes brine to be discharged. Wastewater is then returned post-treatment and combined during PRO with the brine discharge to reduce the brine concentration back seawater levels and recover energy from the osmotic pressure gradient.

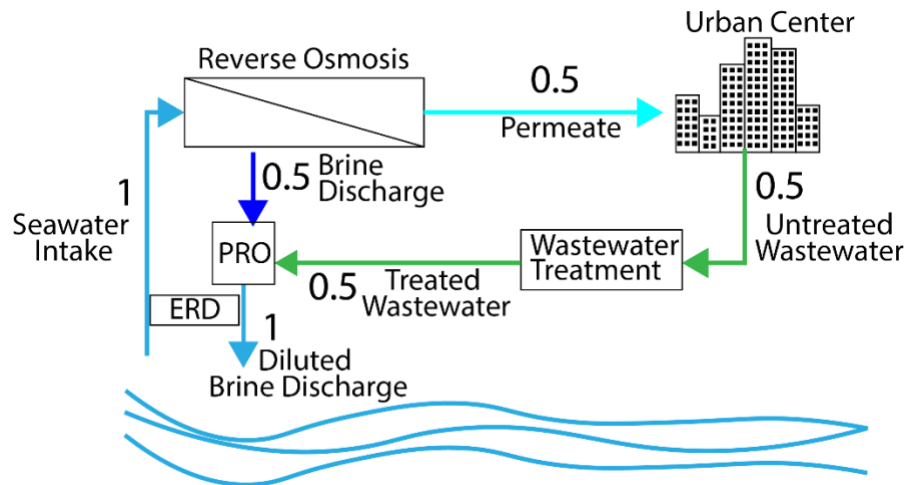


Figure 5. Hypothetical water cycle with RO-PRO process. Values adjacent to the process lines represent the magnitude of flow rate through that particular segment of the process. In this scenario 1 part seawater is split into 0.5 parts permeate and 0.5 parts brine. The resulting

permeate is then utilized by a municipality and recycled through a wastewater treatment plant before returning to be utilized as the feed stream for the PRO process. After PRO blending a diluted brine stream equal in magnitude to the seawater intake is discharged at a concentration approximately equivalent to the surround ocean ecosystem.

Comparing the two hybrid systems, it can be summarized that an FO-RO system has a primary goal of reducing total energy input into the system (minimizing exergy) whereas the RO-PRO system captures and recycles energy within the system (exergy efficiency). There is also a difference in the way each system reuses the treated wastewater. The FO-RO system recovers the wastewater and reintroduces it into drinking water system and is a promising avenue for implementing direct potable reuse [43] considering the evidence of high contaminant rejection of the dual-barrier membrane system [9, 10]. Alternatively, the RO-PRO system does not reintroduce the wastewater into the drinking water system which could be advantageous for avoiding public perception issues or legislative barriers.

Noticeably in Figures 4 and 5, the intake and discharge flow rates of the FO-RO system are half that of the RO-PRO system. This is because an FO-RO system captures and recycles the permeate produced, essentially creating a water reuse loop. This would have the practical advantage of dramatically reducing costs associated with intake, discharge, and associated pretreatment.

2.1.FO and PRO process configuration

In general, FO and PRO processes are comprised of many modules. They are initially arranged in series into a single unit to reach a desired water recovery. These units are then reproduced and arranged in parallel to create a process that meets the desired water output.

Recirculation of the feed stream can be used to achieve higher recoveries. By recirculating the feed stream the residence time in the module is longer and more permeate will be recovered, illustrated by Figure 6A. This also has the added effect of reducing the quantity of feed supplied to the process while maintaining a large flow rate inside of the module.

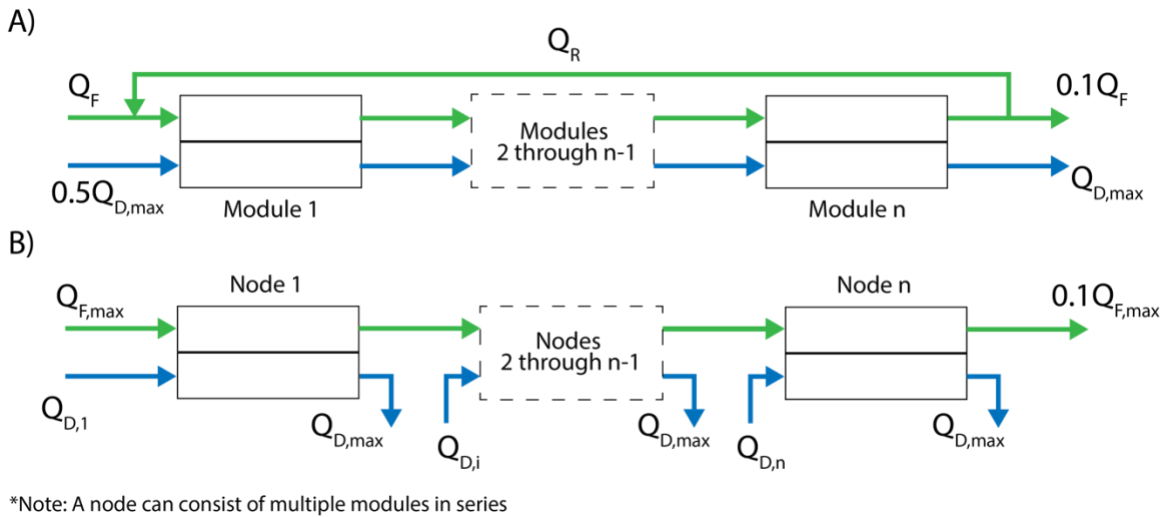


Figure 6. Simplified illustration showing the input and output of the process streams for the A) recirculation configuration and B) recharge configuration

Considering there is a flow rate ratio limitation that is inherent to the spiral-wound membrane design, achieving both the desired recovery and dilution will be impossible for FO and PRO processes by only using the addition of modules in series. A multi-stage recharge configuration, as an alternative to recirculation, is proposed. For the FO process, the draw stream is the limiting quantity that will dictate the amount of the feed stream that will be recovered. By recharging this stream, the driving force can be replenished and additional permeate can be recovered. This recharging can be repeated until the target feed stream recovery is met as shown in Figure 7.

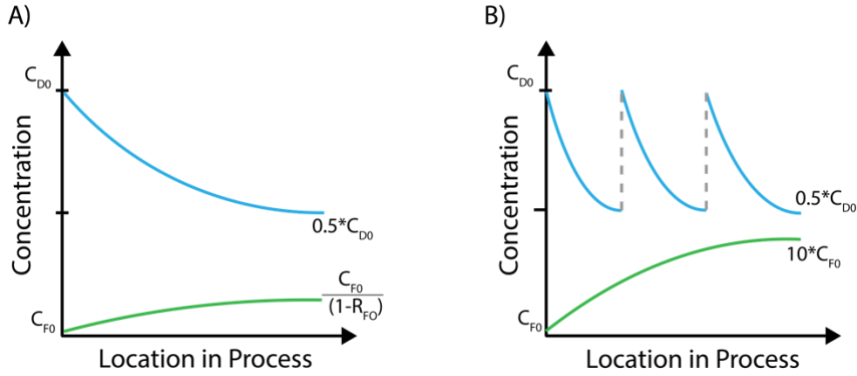


Figure 7. Illustration of the concentrations of both process streams for a A) single-stage non-recharge without recirculation and B) multi-stage recharge configurations for a forward osmosis process as a function of position along the length of the process the process where C_{D0} and C_{F0} are the starting concentration of the draw and feed streams respectively. Since the draw stream recovers an equal volume of permeate, the final concentration is half of the starting value for both configurations. In the A) single stage configuration, the final feed stream concentration is a function of the flow rate ratio (R_{FO}), whereas for the recharge design, with 90% recovery, the final concentration is always 10 times the starting value. The grey dashed lines indicate a recharge of the stream.

It is important to note that when the process without recharge has a large enough recirculation flow rate, the ratio of draw to feed flow rate for the non-recharge process will be equal to the recharge configuration. For example, the recirculation flow rate that is needed to achieve a 0.9 flow rate ratio for both systems is described by Equation 15-17. This recirculation flow rate will be dependent on the module's flow rate ratio (R_{FO}) and the maximum allowable flow rate outside of the envelope, in this case $Q_{F,max}$.

$$Q_R = Q_{F,max}(1 - 0.45R_{FO}) \quad (15)$$

For the process with recharge (B) the amount of feed water is fixed at $Q_{F,max}$ and the total amount of draw utilized by all of the nodes can be described by:

$$\sum_{i=1}^n Q_{D,i} = 0.9Q_{F,max} \quad (16)$$

This assumes each draw stream is diluted with an equal volume of permeate to reach the target dilution. To utilize 90% of the feed water, multiple nodes will be required to recover the necessary amount of permeate. The number of nodes with recharge required depends on the flow rate ratio and can be determined by an integer value of:

$$n = \frac{0.9}{R_{FO}} \quad (17)$$

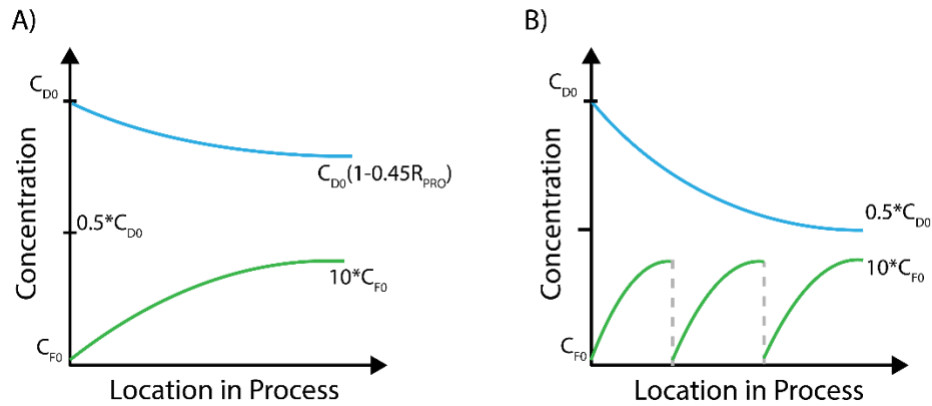


Figure 8. Illustration of the concentrations of both process streams for a A) single-stage non-recharge and B) multi-stage recharge configurations for a pressure retarded osmosis process as they travel along the process where C_{D0} and C_{F0} are the starting concentration of the draw and feed streams respectively. Since the feed stream has a 90% recovery in both configurations, the final concentration is half of the starting value for both designs. In the A) single stage configuration, the final draw stream concentration is a function of the flow rate ratio (R_{PRO}),

whereas for the multi-stage design the final concentration is always half the starting value. The grey dashed lines indicate a recharge of the stream.

Similarly, the PRO process can be arranged in this recharge design to achieve the desired dilution. Illustrated in Figure 8, by periodically recharging the feed stream there is more available permeate for recovery that will allow the PRO process to be diluted. The PRO process does not use recirculation on the feed side because as the flow rate on the feed side is the smallest, recirculation would reduce the amount of permeate that could be recovered. A similar two-stage configuration has been studied using a mathematical approach by He et al. [44] and was found to be a promising improvement in total energy recovery over a single PRO module. This work expands on that premise and explores a much larger multi-stage PRO process with direct application to spiral-wound modules using numerical modeling.

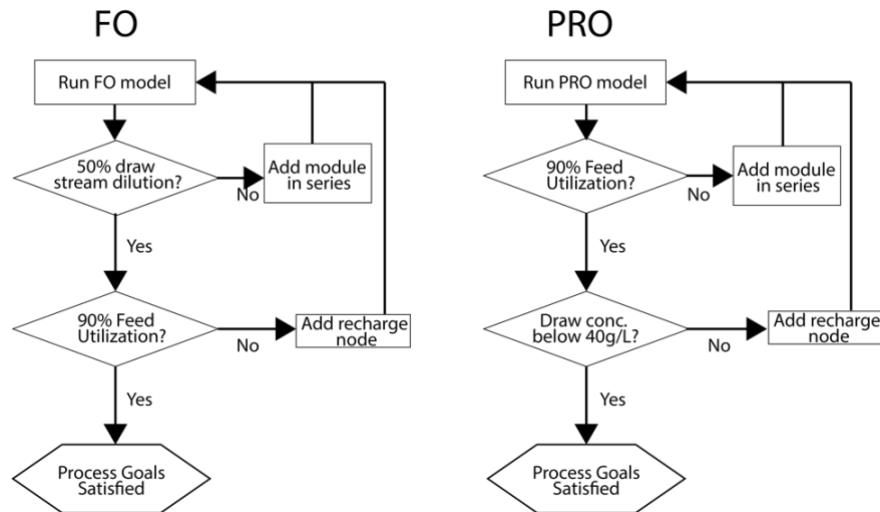


Figure 9. Model logic flow chart for FO and PRO. This logic controls when to add an additional module or node to achieve process goals.

To find the recharge configuration for FO requiring the least number of membranes, the model solver begins with one module and if the desired draw dilution is not reached, an additional module is added. Once the desired draw stream dilution is reached, the feed water utilization is assessed as illustrated in Figure 9. If the utilization has not met the desired target, an additional node is added. In FO, the addition of a node consists of discharging the diluted draw stream and recharging the draw stream as shown in Figure 10. The 50% dilution condition is then applied to the new node and additional modules are added. The logic scheme is repeated until both conditions are simultaneously satisfied. Considering the draw stream is often operated at a much lower flow rate than the feed stream, this results in low permeate recovery and the requirement of multiple nodes is likely. The arrangement with multiple nodes and the replenishment of the stream inside of the envelope, will be referred to as the “recharge configuration” in contrast to a simple arrangement of modules without the addition of nodes as the “non-recharge configuration”.

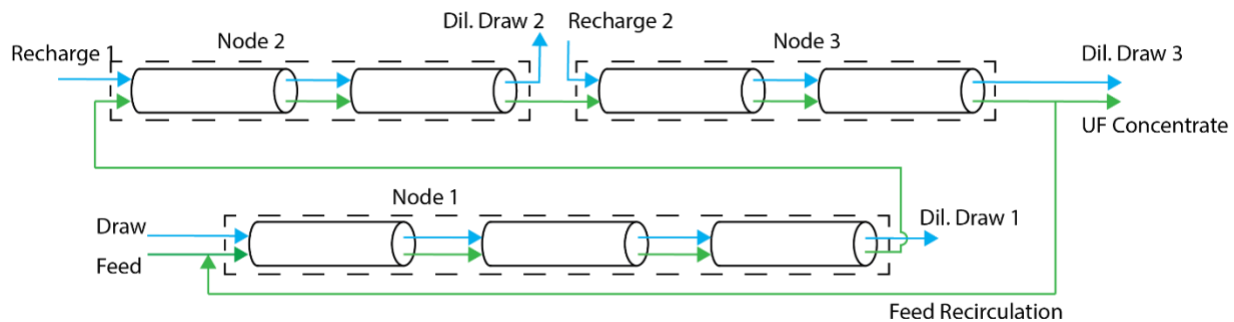


Figure 10. Illustration of the proposed configuration for an FO unit process. The key feature to note is the periodic discharge and recharge of the draw stream within a single unit.

Similarly, PRO requires the addition of multiple modules in series to achieve high utilization of the feed stream. Considering the modules have limited flow rates on the feed side, a single

feed stream can't achieve the desired dilution of the brine stream. This is solved by recharging the feed stream periodically. The process is initialized with a single module and additional modules are added in series until the feed utilization has reached 90% as illustrated in Figure 9. Once the utilization target is met, the discharge concentration is evaluated. If the discharge concentration isn't below the designated 40 g/L limit, an additional node is added. For PRO, the addition of a node consists of discharging the reject stream and recharging the feed stream as shown in Figure 11. As previously stated, for PRO, the model does not adjust the recirculation on the feed side therefore the PRO process relies solely on the addition of modules to increase the recovery of the feed stream.

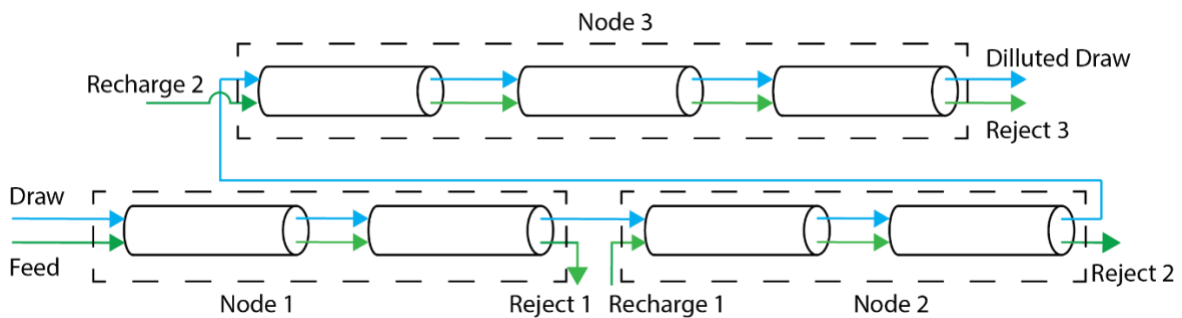


Figure 11. Illustration of the proposed configuration for a PRO treatment train. The key feature to note is the periodic discharge and recharge of the feed stream within a single train.

2.2. Module geometry

The module geometry is representative of a spiral-wound membrane module that would be used in an industrial setting. This type of module is an 8040 spiral-wound element composed of a central permeate tube with a membrane rolled around it. The important aspects of the module to consider are the module dimensions, membrane characteristics, flow conditions, number of leaves, and membrane baffling.

Membrane characteristics for this study are listed in Table 1 and were selected based on values used in literature. The notable membrane characteristics are the water permeability coefficient (A), salt permeability coefficient (B), membrane length, membrane width, membrane thickness, and the structural parameter. It is worth noting that these are starting values, as sensitivity analyses were performed varying the water permeability coefficient, salt permeability coefficient, and channel height.

Table 1. Membrane parameters used in modeling

Parameter	Units	Value	Ref.
Water permeability coefficient	m/s kPa	1.42×10^{-8}	[25]
Salt permeability coefficient	m/s	2.41×10^{-8}	[25]
Structural parameter	m	3.1×10^{-4}	[25]
Length of membrane	m	1.016	[25]
Total membrane area	m ²	14.4	[45]
Channel Height	m	8.0×10^{-4}	[25]
Number of leaves		9	[25]
Maximum flow rate inside envelope	LPM	140	[25]

In spiral-wound modules, multiple membrane leaves are attached to the central permeate tube as a way of dividing the flow and total membrane area into several elements and increase packing density. The number of leaves is important but considering each leaf has identical membrane characteristics and inlet flow conditions, a single leaf can be modeled, and the resulting flow rates multiplied by the number of leaves achieves the total flow rate of the entire module. As the mass transfer and flow behavior are not affected by the curvature of the channel, the membrane can be considered unrolled and modeled as a flat sheet.

Baffling is used to lengthen the flow path inside of the envelope and increase the contact time between the two streams for increased recovery. As the exact hydrodynamic behavior of the flow around a baffle is quite complex for a numerical model, it must be simplified. This aspect

is simplified by extending the baffle to the edge of the membrane and then reflecting the flow across the baffle axis as shown in Figure 12.

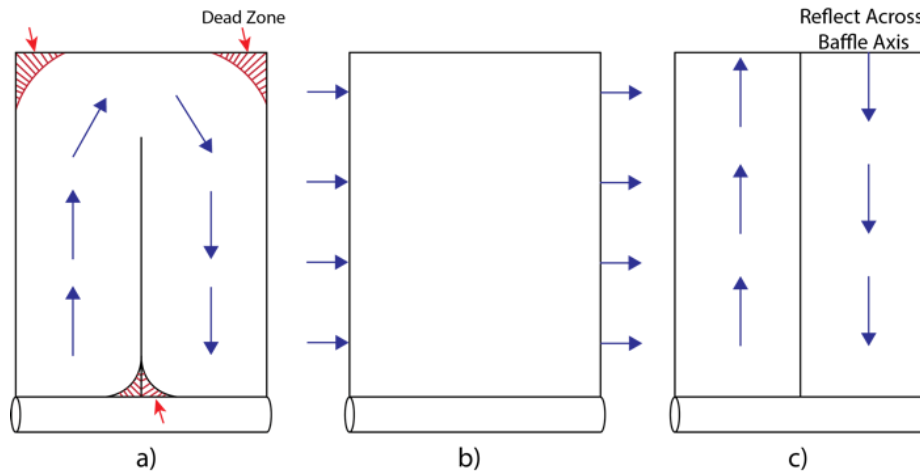


Figure 12. a and b) Illustration of a realistic flow path in a spiral-wound membrane. c) Simplified flow path for modeling purposes. The “dead zones” highlighted in the realistic representation would be far too rigorous to accurately model with a numerical method. By simplifying the flow domain makes a numerical model possible without losing as much accurate representation as a plate and frame model does.

2.3. Module discretization

2.3.1. Iteration Scheme

To project the performance of the module accurately, the computational domain was discretized into differential lengths and widths where the solver could be applied. It is a common technique to discretize in a linear approach and iterate along the membrane as shown in Figure 13 [35, 42, 46-48]. However, this doesn't accurately represent the cross-flow operation and should be improved upon. The iteration methodology used in this work was developed to best replicate the cross-flow configuration shown by Figure 14.

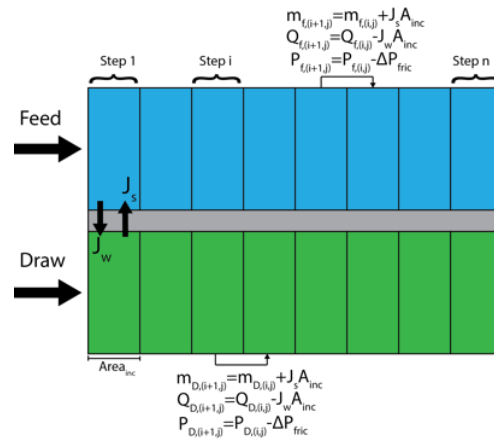


Figure 13. Iteration scheme of a plate and frame model. The streams interactions can be either co-current or counter-current and are updated sequentially.

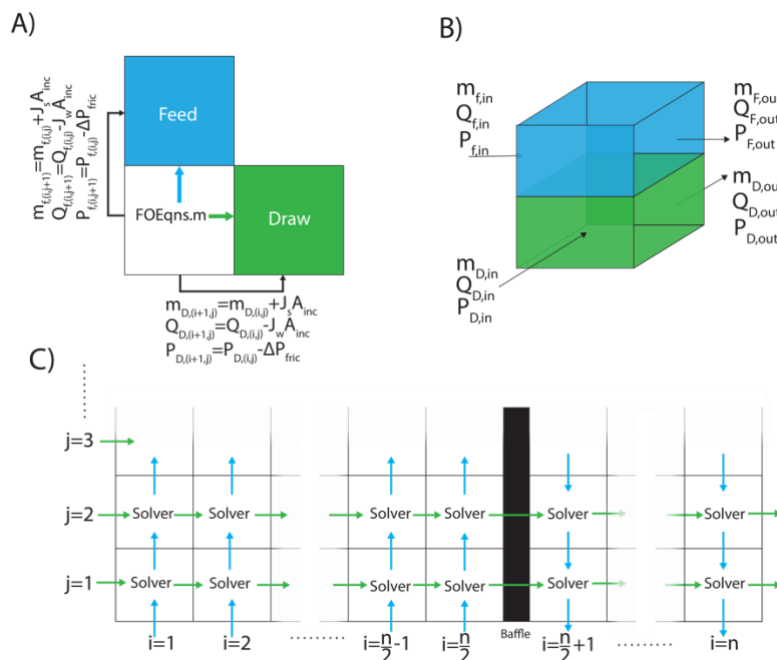


Figure 14. Iteration scheme and arrangement of a “cross-flow” model and how A) the model is applied for accurate stream interaction and information propagation from the discretized area. This scheme more accurately represents the B) orthogonal relationship between the feed and draw side channels. C) The model application is iterated in a way to represent the flow path of both streams with consideration to the presence of the baffle. This feature is important as the

baffle has a large impact of volumetric flow rate and lengthens the total flow path of the channel it is located in.

The water flux, salt flux, and pressure losses are solved at each differential area based on the values entering the cell and used to update the value of the variable exiting the cell. The equations describing the updated variables are:

$$Q_{D,out} = Q_{D,in} + J_w A_{inc} \quad (1)$$

$$Q_{F,out} = Q_{F,in} + J_w A_{inc} \quad (2)$$

$$m_{D,out} = m_{D,in} + J_s A_{inc} \quad (3)$$

$$m_{F,out} = m_{F,in} + J_s A_{inc} \quad (4)$$

$$P_{D,out} = P_{D,in} - P_{D,loss} \quad (5)$$

$$P_{F,out} = P_{F,in} - P_{D,loss} \quad (6)$$

$$P_{loss} = \frac{\lambda \rho v^2 L}{2d_h} \quad (7)$$

where λ is the friction coefficient, ρ is the density of the fluid, v is the velocity of the fluid, L is the length of the channel and d_h is the hydraulic diameter defined by:

$$d_h = \frac{2Wh_{chan,eff}}{W+h_{chan,eff}} \quad (8)$$

where W is the channel width and $h_{chan,eff}$ is the effective channel height which is the actual channel height minus the diameter of any spacer present in the channel.

2.3.2. Governing Equations

The fundamental equations for water flux and reverse solute flux across a membrane are described by:

$$J_w = A(\Delta\pi - \Delta P) \quad (9)$$

$$J_s = B\Delta C \quad (10)$$

where J_w is the water flux, $\Delta\pi$ is the osmotic pressure differential, ΔP is the hydraulic pressure differential, J_s is the reverse solute flux, and ΔC is the concentration differential. However, due to the asymmetric structure of the membrane and differences between the rates of mass transfer and diffusion, the osmotic pressures experienced by the active layer of the membrane are different from that of the bulk. To accurately model the mass transfer, the model must account for concentration polarization within the membrane and the boundary layer.

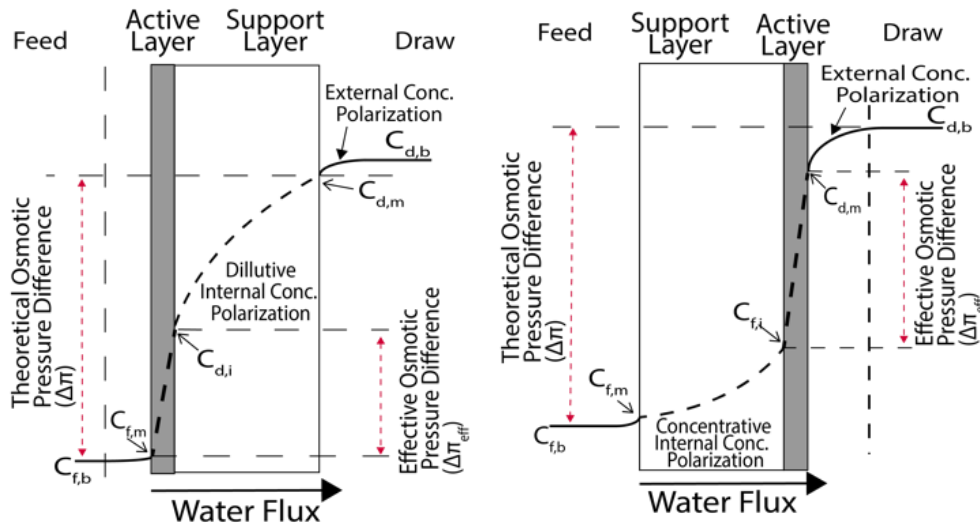


Figure 15. (Left) Membrane arrangement and concentration profile for an FO process.

The figure provides clarity to the magnitude difference of both the internal and external concentration polarizations. In FO, the ICP is more significant than in PRO (Right) Membrane arrangement and concentration profile for a PRO process

Figure 15 illustrates the concentration profiles in both FO and PRO processes. The type of concentration polarization experienced inside the membrane and flow channel depends on the operation mode. Both FO and PRO experience concentrative ECP in the feed stream and dilutive ECP in the draw stream. However, inside the support layer of the membrane, FO

experiences dilutive ICP while PRO experiences concentrative ECP. When the equations for concentration polarization are coupled into the flux equation for FO & PRO, the resulting equations are thus [49, 50]:

$$J_w = A \left[\frac{\pi_{D,b} \exp(-J_w K) - \pi_{F,b} \exp\left(\frac{J_w}{k}\right)}{1 + \frac{B}{J_w} \left[\exp\left(\frac{J_w}{k}\right) - \exp(-J_w K) \right]} \right] \quad (11)$$

$$J_s = B \left[\frac{C_D \exp(-J_w K) - C_F \exp\left(\frac{J_w}{k}\right)}{1 + \frac{B}{J_w} \left[\exp\left(\frac{J_w}{k}\right) - \exp(-J_w K) \right]} \right] \quad (12)$$

$$J_w = A \left[\frac{\pi_{D,b} \exp\left(-\frac{J_w}{k}\right) - \pi_{F,b} \exp(J_w K)}{1 + \frac{B}{J_w} \left[\exp(J_w K) - \exp\left(-\frac{J_w}{k}\right) \right]} - \Delta P \right] \quad (13)$$

$$J_s = A \left[\frac{C_D \exp\left(-\frac{J_w}{k}\right) - C_F \exp(J_w K)}{1 + \frac{B}{J_w} \left[\exp(J_w K) - \exp\left(-\frac{J_w}{k}\right) \right]} \right] \quad (14)$$

where Equations 11 & 12 describe the water and salt flux for FO and Equations 13 & 14 describe the same for PRO. These equations include the mass transfer coefficient (k) and the solute resistivity for diffusion within the porous support layer (K) which are necessary for describing the concentration profile resulting from the polarization effects.

The power density and the specific energy recovery (SER) of the PRO process are evaluated at the end of the process. The gross specific energy recovery (SER) is the gross energy produced by the PRO process and can be calculated by:

$$SER \left(\frac{kWh}{m^3} \right) = \frac{Q_{P,PRO} P_{D,out}}{Q_{RO}} \quad (15)$$

where $Q_{P,PRO}$ is the permeate flow rate across the membrane, Q_{RO} is the permeate production flow rate of any integrated RO process (which is equal to the brine flow rate), and $P_{D,out}$ is the outlet pressure of the PRO draw stream. The gross SER does not account for the pumping energy used by the pumps for circulating the fluid streams. The energy requirement to overcome

the pressure loss experienced in the module is calculated and subtracted from the gross SER to provide an estimate for net SER, shown by Equation 16:

$$SER \left(\frac{kWh}{m^3} \right) = \frac{Q_{P,PRO} P_{D,out}}{Q_{RO}} - Q_D \Delta P_D - Q_f \Delta P_f \quad (16)$$

where Q_D and Q_f are the flow rates on the draw and feed side of the membrane respectively and ΔP_D and ΔP_f are the pressure losses experienced on the draw and feed side of the membrane respectively. The power density is calculated by:

$$W = \frac{SER * Q_{RO}}{A_{mem}} \quad (17)$$

where A_{mem} is the total membrane area used by the process.

Flow rate ratios

The model is used to quantify the effect that the imbalance in flow rates in a spiral-wound module has on FO and PRO operation. The “flow rate ratios” (R_{FO} and R_{PRO}) are defined as:

$$R_{FO} = \frac{Q_{DS}}{Q_{FS}} \quad (18)$$

$$R_{PRO} = \frac{Q_{FS}}{Q_{DS}} \quad (19)$$

where Q_{DS} is the flow rate on the draw side and Q_{FS} is the flow rate on the feed side. The modules selected for modeling have a manufacturer suggested maximum operating flow rate on the higher flow rate side of 140 LPM. This will be the maximum flow rate setting for the feed side in FO, and conversely, the draw side in PRO.

To illustrate the difference in the SER between plate-and-frame and spiral-wound modules, a survey on the impact of effective channel height and flow rate ratio on the SER for a single module operating in PRO is done. Altering the effective channel height is used to survey the

pressure loss impact on SER. The effective channel height is an efficient independent variable as it accounts for any change in both the actual channel height or spacer size and will directly affect the pressure loss as shown in Equations 7 and 8. For both modules types, the effective channel height will be varied from 0.6 mm to 1.8 mm in increments of 0.2 mm and the flow rate ratio will be varied between 0.1 and 0.9 in increments of 0.1.

Additionally, the impact of different flow rate ratios and channel heights on SEC and SER of FO and PRO is compared between recharge and non-recharge configurations. For both FO and PRO processes, the effective channel height is again varied from 0.6 mm to 1.8 mm and the flow rate ratio will be varied between 0.1 and 0.9.

To determine if the recharge configuration offers any advantage in PRO compared to the non-recharge configuration over a range of membrane properties, a survey on the effect of water and salt permeability is done. The permeability characteristics are varied and tested for configurations with and without recharge. The water permeability is varied from 1×10^{-8} m/s kPa to 1×10^{-6} m/s kPa and salt permeability is varied from 1×10^{-8} m/s to 1×10^{-6} m/s.

3. Results

3.1. Plate and Frame vs Spiral-Wound

The difference in PRO net SER between plate and frame and spiral-wound is shown in Figure 16. This figure highlights the difference in the effect of channel heights and flow rate ratios on net SER between A) plate-and-frame (PF) and B) spiral-wound setups. Each module type was tested with flow rate ratios between 0.1 and 0.9. Additionally, the effective channel height was varied between 0.6 mm and 1.8 mm. The SER was found to be between 0.03 kWh/m³ and 0.11 kWh/m³ for the plate-and-frame module and 0.06 kWh/m³ and 0.12 kWh/m³ for the

spiral- wound module. Both module types exhibit the highest net SER at a channel height of approximately 0.8 mm. This is likely due to reduced ECP and ICP as a result of higher channel velocities compared to channel heights above 0.8 mm. Conversely, channel heights below 0.8 mm experience higher pressure losses due to high velocities, requiring a larger energy demand to overcome these pressure losses, effectively reducing the net SER.

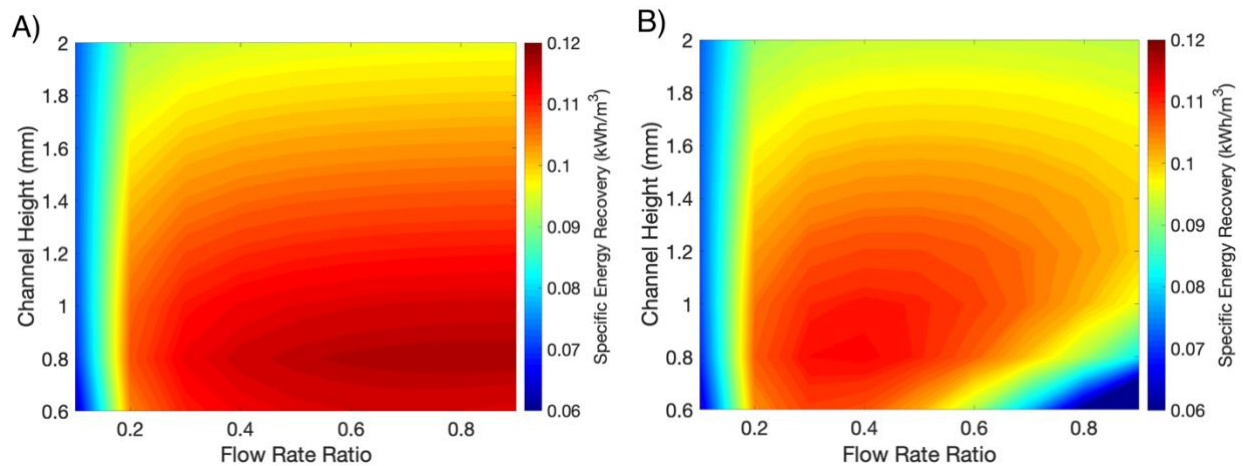


Figure 16. Contour plot illustrating the effect of flow conditions on the specific energy recovery for A) a single plate and frame module and B) a single spiral-wound module. The flow rate ratio was varied between a 0.1 to 0.9 feed to draw ratio. Additionally, the height of the channel for both the draw and feed streams was varied between 0.6 mm and 2 mm.

The two module types differ most in their response to changes in the flow rate ratio. Plate-and-frame modules have better SER as the ratio approaches 0.9. This is because the hydraulic resistances of the draw and feed channels are approximately the same in the PF modules and results in each channel experiencing roughly equal pressure drops. As a result, equal draw and feed flow rates can be processed by the module without greatly affecting the driving force due to

imbalances in pressure build up between the two channels, resulting in more permeate to being recovered at higher flow rate ratios.

The SW module is found to have the highest SER at a flow rate ratio of approximately 0.35. At high flow rate ratios, the increased pressure losses inside of the envelope results in a large energy requirement for pumping effectively reducing the SER. This can also be assumed to be analogous to an increased SEC for FO. The lower SER at high flow rate ratios is a significant outcome because it demonstrates the inability of a spiral-wound module to process an equal amount of feed and draw flow rates in an efficient manner.

3.2. Configuration sensitivity to changes in operating conditions

Forward Osmosis

Non-recharge without recirculation

Figure 17A shows the FO wastewater utilization as function of channel height and feed/draw ratio. The lowest utilization achieved was as low as 5.9% with the highest value reaching 22.9%. Overall, utilization with this configuration is poor and far short of the desired 90%. The flux termination point was reached very early at the higher flow rate ratios due to the increase pressure in the draw stream channel which limited the recovery when there was still an osmotic pressure difference available. Conversely, at the lower flow rate ratios the draw stream would reach the target dilution before recovering a significant amount of the feed stream. The specific energy consumption is shown in Figure 17B. The flow rate ratio was varied between 0.1 and 0.9 to test the response to the amount of draw stream processed by the configuration and the channel height was varied between 0.6 mm and 1.8 mm to stress the process response to pressure loss. The results showed a range of SEC between 1.1×10^{-3} kWh/m³ and 0.25 kWh/m³. The SEC only reaches high values when the channel height is below 0.8 mm and the flow rate ratio is above

0.8. The resulting RO influent concentration achieved by the process is illustrated in Figure 17C. The resulting RO influent concentrations for this configuration has a range of 15.3 g/L to 28.6 g/L. The desired dilution is not always achieved as the flux termination is prematurely reached as the flow rate ratio approaches 0.9 which is a direct result from the increased pressure in the draw channel from the higher flow rates. Figure 17D shows the average flux for the process. The range of average flux for all conditions tested ranges between 5.3 LMH to 13.4 LMH.

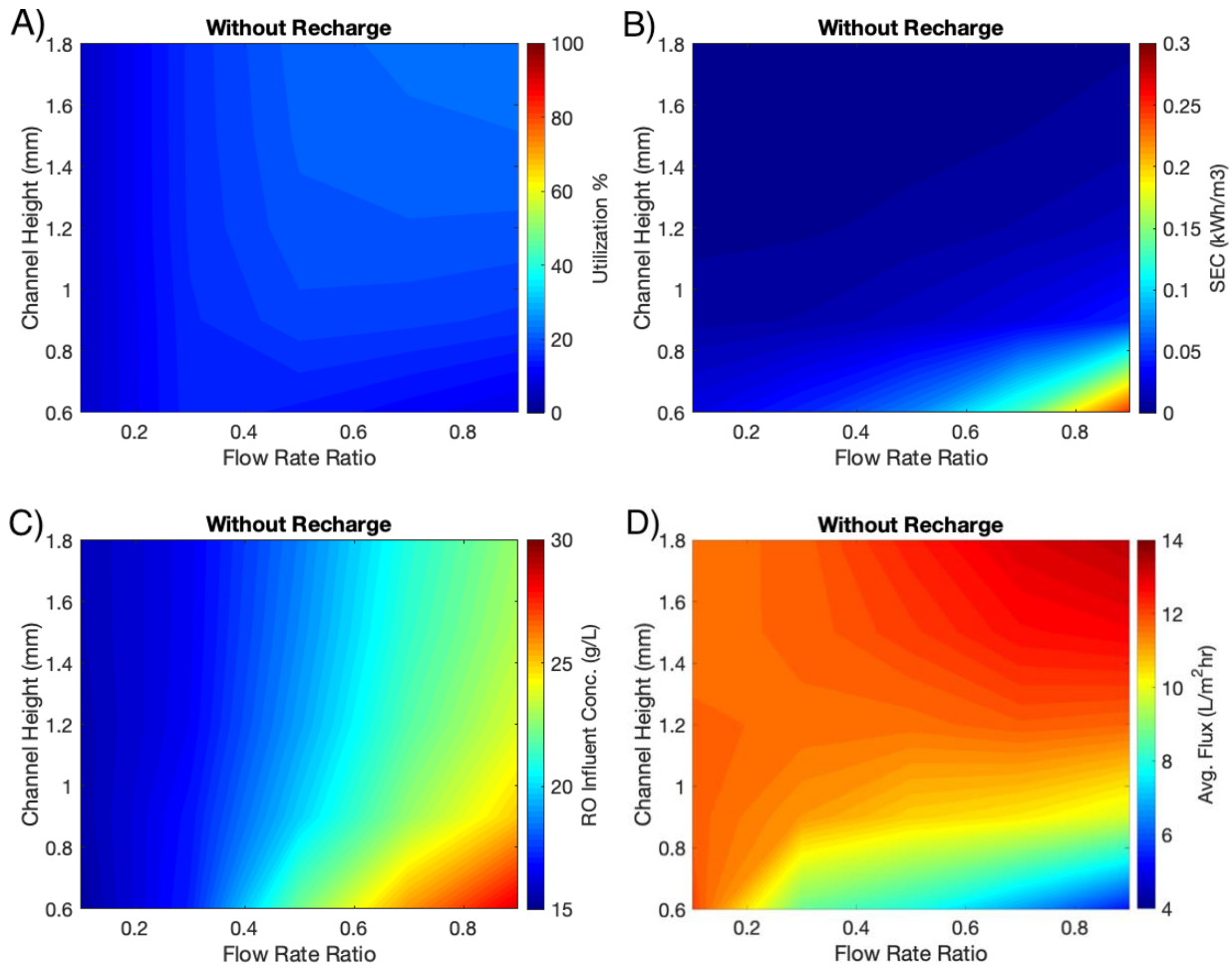


Figure 17. Contour plots illustrating the A) feed utilization, B) specific energy consumption, C) RO influent concentration, and D) average flux the for the FO process without recharge or recirculation. In these simulations the flow rate ratio was varied between a 0.1-0.9 feed to draw ratio and the height of the channel for both the draw and feed streams was varied between 0.6mm

and 2mm. A 90% feed stream recovery target was implemented to minimize the amount of treated wastewater unutilized, however, in some cases the flux termination point was reached prematurely.

Non-recharge with recirculation

Figure 18A shows that higher utilization can be achieved with the use of recirculation of the feed stream. This allows the FO process without recharge to recover a much greater amount of permeate with a range of 16.7% to 96.3%. Figure 18B shows the effect of the flow rate ratio and channel height for this process. The values for the SEC were found to be between 1.0×10^{-3} kWh/m³ and a high of 0.39 kWh/m³. As expected, the energy consumption is greatest at large flow rates and low channel heights. These values are in agreement with an experimental studies for an FO process with multiple 8040 spiral-wound modules in series recovering up to 90% of the available feed that showed an SEC of approximately 0.2 kWh/m³ [10]. Figure 18C shows the resulting RO influent concentrations where the range of values for all scenarios are between 15.1 g/L to 29.0 g/L. This is analogous to the process without recirculation since recirculation only increases the utilization but does nothing to increase total permeation. In fact, there should be a slight decrease due to the higher average feed concentration due the recirculation of solutes. This is seen in Figure 18D which shows the average flux for the process. The range of average flux for all conditions tested ranges between 3.2 LMH to 12.4 LMH. The FO configuration with recirculation has a noticeably lower average flux than the FO configuration without recharge or recirculation. This means that for the higher utilization will require an increased capital cost.

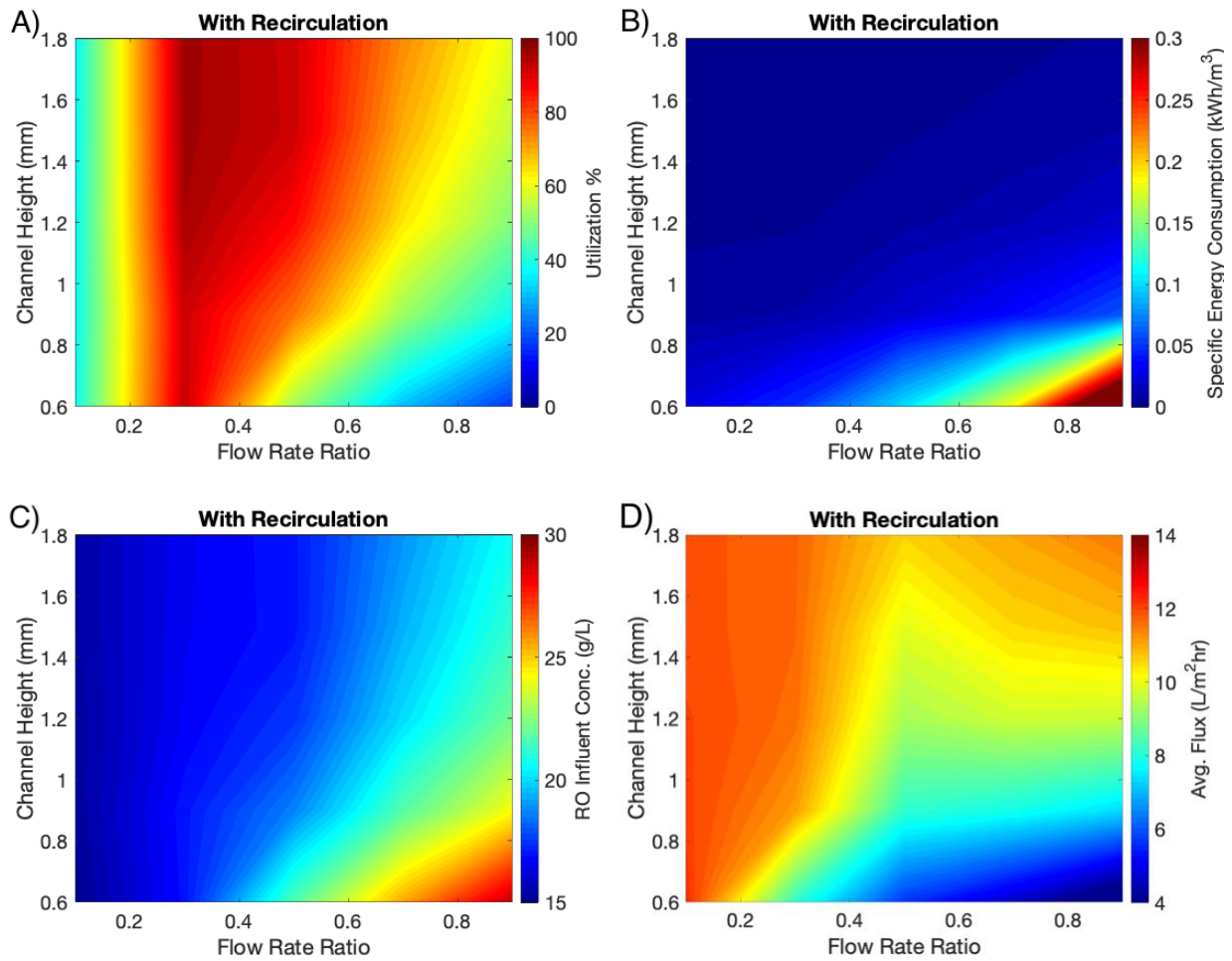


Figure 18. Contour plots illustrating the A) feed utilization, B) specific energy consumption, C) RO influent concentration, and D) average flux the for the FO process without recharge with the use of recirculation.

Recharge

Figure 19A shows that recharging the draw stream results in a significant increase of FO process performance in terms of total wastewater utilization. The use of recharge allows the FO process to recover a much greater amount of permeate with a range of 90.0% to 91.5%. This is a much more stable configuration with a much smaller range of utilization. Despite an increase in recovery performance, there is no trade-off with energy consumption. The SEC results are

shown in Figure 19B and were found to be between 3.7×10^{-4} kWh/m³ and a high of 0.25 kWh/m³. This configuration shows lower specific energy consumption than the recirculation configuration and identical energy consumption to the non-recharge. This configuration requires many more membranes than the recirculation configuration, which results in greater energy consumption due to increased pressure losses, but when normalized to the permeate production the specific energy consumption for this process configuration is more favorable because the total permeate recovery is also much greater and increases at a greater rate than the energy consumption.

The resulting RO influent concentrations are shown in Figure 19C. The RO influent concentrations for all conditions are between 16.1 g/L to 29.2 g/L. The results show that at larger flow rate ratios the flux termination point was reached prior to the desired dilution of the draw stream. For either process configuration, operating at a lower flow rate ratio is advantageous and will result in a more desirable RO influent stream. This system performs similar to the other two. Figure 19D show the average flux during operation at large flow rate ratios and small channel heights is inefficient similarly to the other configurations. The range of average flux for all conditions tested ranges between 3.7 LMH to 11.9 LMH. The average flux for this configuration was lower than both the recirculation configuration and the non-recharge, which suggests this configuration requires a compromise from a membrane area efficiency standpoint to achieve high utilization.

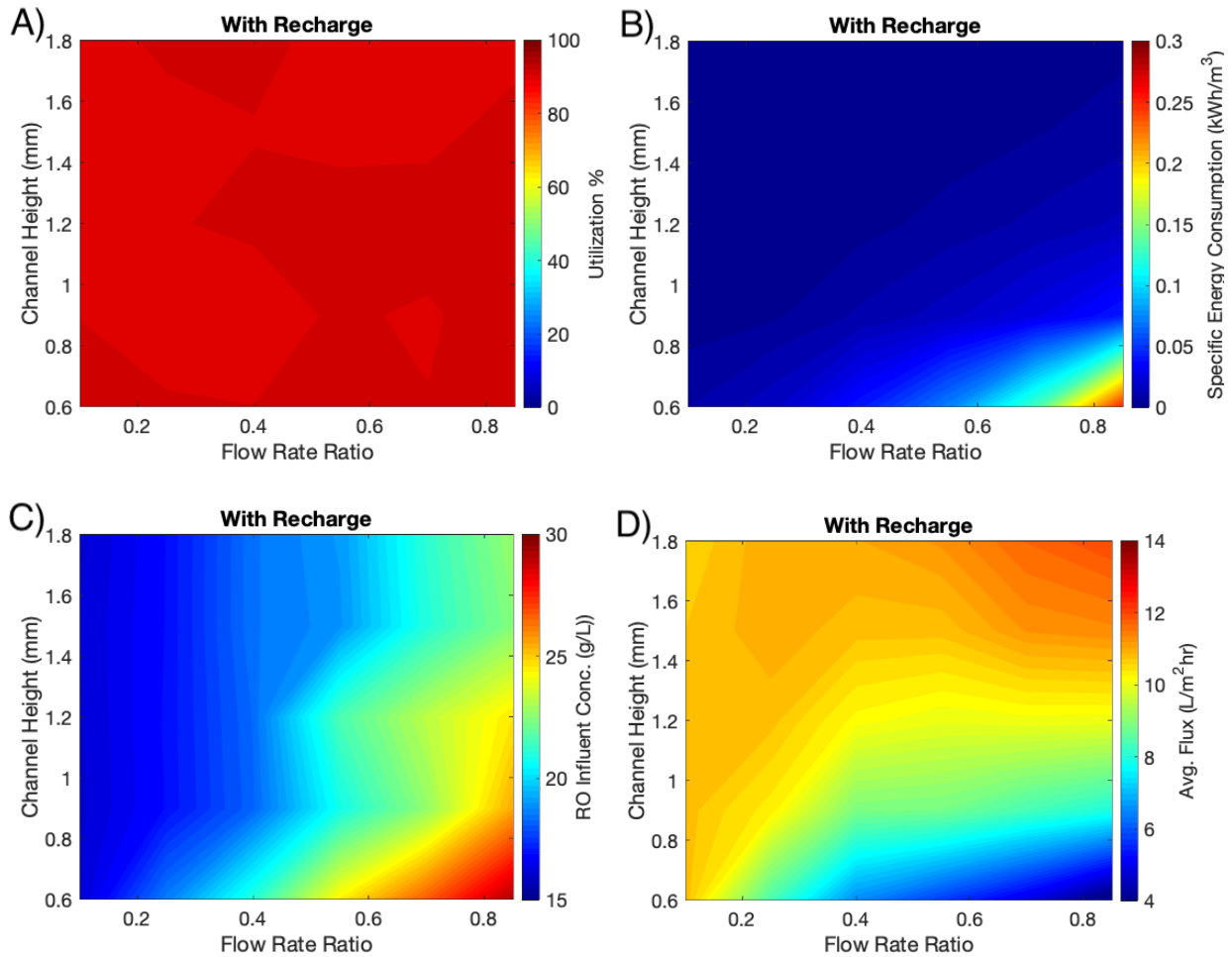


Figure 19. Contour plots illustrating the A) feed utilization, B) specific energy consumption, C) RO influent concentration, and D) average flux the for the FO process with recharge.

Pressure Retarded Osmosis

Figure 20A illustrates the performance behavior of a PRO process without recharge. The flow rate ratio is the primary driver for energy recovery with values for this configuration ranging from 0 kWh/m³ to 0.45 kWh/m³. As the flow rate ratio approaches 0.9, the efficiency of the membrane decreases but the overall permeate recovery is larger and as a result the overall SER is greater. The Figure does show that increased channel height begins to have a positive effect on energy recovery at the higher flow rate ratios. At these larger flow rates there may be a

positive trade-off with increasing concentration polarization to alleviate some of the pressure losses. Conversely, Figure 20B shows that for the configuration with recharge, the flow rate ratio is not significantly influential to energy recovery. This is because once the initial amount of feed water is 90% recovered, additional streams of feed water can be introduced until the draw stream reaches the desired discharge concentration. As a result, a consistent amount of permeate and energy is recovered across all flow rate ratios.

This is the key result of the recharge configuration for PRO. By recovering the same amount of permeate for all module flow rate ratios, the overall process can perform at a high net SER regardless of module limitations. This showcases the adaptability of the recharge configuration to mitigate the imbalanced pressure losses of the two channels of the membrane.

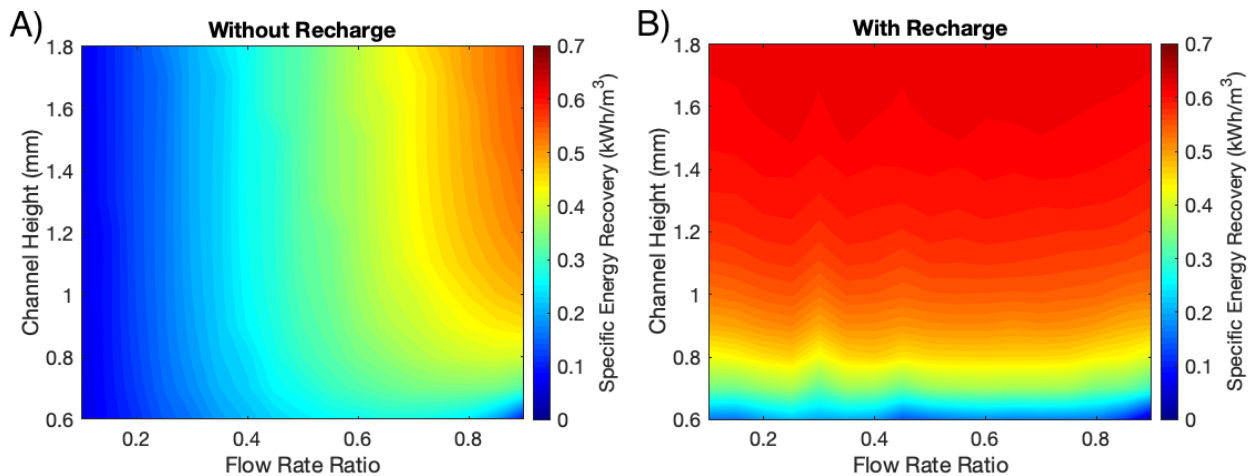


Figure 20. Contour plot illustrating the effect of flow conditions on the specific energy recovery of a PRO process. A) Results for a PRO process arranged in a series configuration without recharge. B) Results for a PRO process arranged in a series configuration with recharge. The membrane properties for both simulations are listed in table 1. In these simulations the flow rate ratio was varied between a 0.1-0.9 feed to draw ratio and the height of the channel for both the

draw and feed streams was varied between 0.6mm and 2mm. A 90% feed stream recovery target was implemented to minimize the amount of treated wastewater unutilized.

For both of these configurations, increasing the channel height will increase the specific energy recovery. The results for the recharge configuration agree with Figure 20A that at larger flow rates the channel height has an increased effect on energy recovery. Even though the feed flow is split into multiple nodes, the effective energy required to overcome the combined pressure losses of the total flow rate for all of the nodes is similar to the configuration without recharge at a higher flow rate ratio. Again, this suggests that there may be a positive trade-off by increasing channel height. However, there is a limitation to increasing channel height as the concentration polarization will begin to dominate the driving force for water flux.

Figure 21 illustrates the results of how membrane characteristics affect the specific energy recovery for the two types of process configurations. In these simulations, the channel height is set to 0.8 mm and the flow rate ratio is fixed at 0.3 based on the best operating conditions indicated in Figure 16B. The results for the configuration without recharge show that the water and salt permeability coefficients don't greatly affect the energy recovery of the process. Since the flow rate ratio for this experiment is set at 0.3, the draw stream can effectively recover 90% of the feed water even with non-ideal membrane properties because the larger amount of draw maintains the driving force throughout the process. As a result, the SER only varies between 0.1 kWh/m³ and 0.13 kWh/m³. Although this process has stable performance for a range of membrane properties, this process is greatly limited in its maximum energy recovery potential compared to the configuration with recharge. Figure 21B illustrates that the configuration with recharge is much more sensitive to changes in the permeability of the membrane but can achieve a much greater energy recovery. For this configuration, the specific energy recovery ranges from

0 kWh/m³ to 0.55 kWh/m³ whereas the configuration without recharge only varies between 0.1 kWh/m³ and 0.13 kWh/m³. Considering the recharge configuration is designed to recover the same amount of permeate for all conditions, the gross SER will always be the same regardless of membrane characteristics. However, for a membrane with low water permeability, there will be a greater number of membranes required, increasing the SEC and reducing the net SER. Figure 21 shows that the resulting increased SEC at lower water permeabilities has much more drastic impact on the net SER for the recharge configuration compared to the non-recharge.

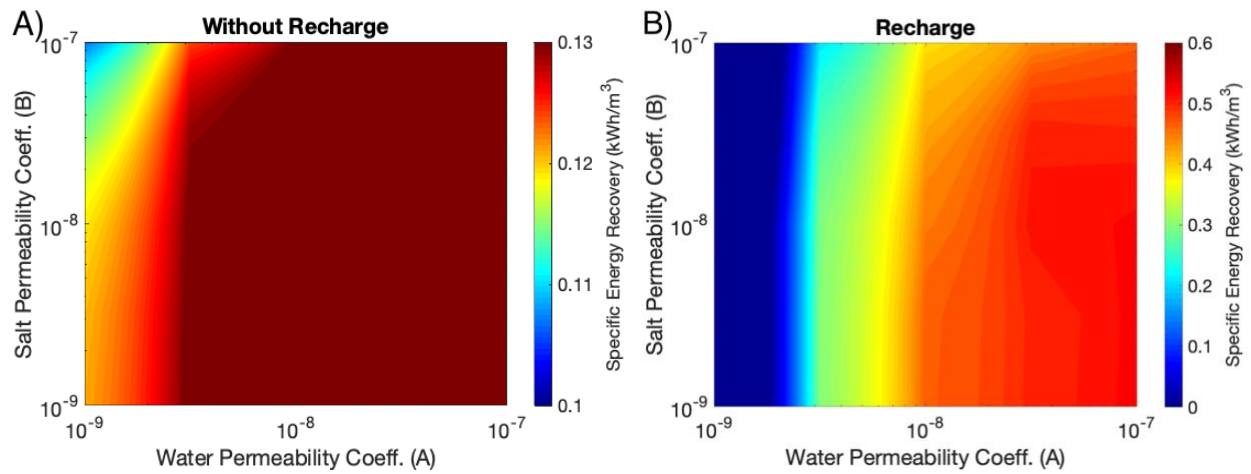


Figure 21. Contour plots illustrating the effect of membrane characteristics on the specific energy recovery of a PRO process. A) Results for a PRO process arranged in a series configuration without recharge. B) Results for a PRO process arranged in a series configuration with recharge. The conditions for both simulations were a 1:5 feed to draw flow rate ratio with the membrane properties listed in table 1. The configuration with recharge is operated to 90% recovery and the configuration without recharge is operated up to the flux termination point.

Figure 22 shows the power density of the PRO process. The non-recharge configuration has a power density range of 2.5 – 10.7 W/m² and the recharge configuration has a power density

range of 0.9 – 9.6 W/m². The results for the non-recharge shows that the power density of the non-recharge configuration is as high as 10.7 W/m² and is relatively consistent for the membrane characteristics tested. Although the range of values are similar, the power density for the recharge configuration is significantly lower for most membrane characteristics tested compared to the non-recharge configuration. The recharge configuration has a power density comparable to the non-recharge configuration only when the membrane has a high water permeability coefficient. This means that although the recharge configuration is much more effective in terms of energy recovery, it is less efficient with a lower power density unless the membrane characteristics are very favorable. This is in agreement with the rationale that for PRO, the objectives of maximizing power density and maximum energy extraction are not mutually attainable. The inverse relationship between effectiveness and efficiency demonstrated in Figure 3 and is true for the recharge configuration.

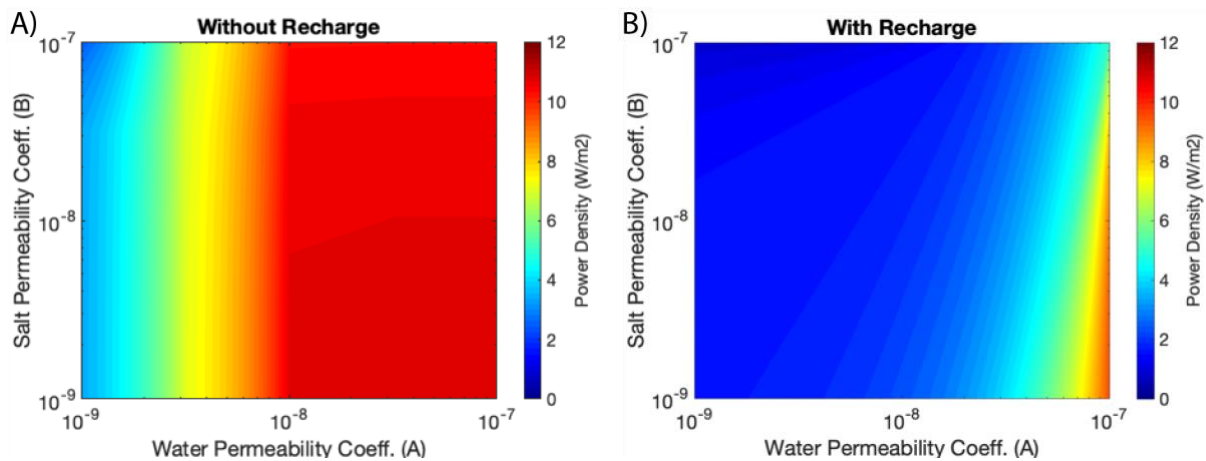


Figure 22. Contour plots illustrating the effect of membrane characteristics on the power density of a PRO process. A) Results for a PRO process arranged in a series configuration without recharge. B) Results for a PRO process arranged in a series configuration with recharge. The conditions for both simulations were a 1:5 feed to draw flow rate ratio with the membrane

properties listed in table 1. The configuration with recharge is operated to 90% recovery and the configuration without recharge is operated up to the flux termination point.

4. Conclusions

Both PRO and FO benefit from the recharge configuration. For FO, utilizing recharge shows improvements in feed water utilization over a single stage configuration even when recirculation is used to compensate for difference in allowable flow rates inside and outside of the envelope. Both the recharge and recirculation configuration achieved the desired utilization at low to moderate flow rates, but utilizing recharge has a distinct advantage at high flow rate ratios. This means that the process will be able to account a variety of draw and feed flow rates without a sacrificing performance. The recharge configuration also showed better average water flux which may lead to lower capital cost investments required for the implementation of the process.

PRO has a distinct advantage from recharging the feed stream due to the greater amount of available permeate for recovery which directly results in more energy recovery. This higher energy recovery comes at a cost of more total membrane area required. Due to requirement of a larger membrane area, the recharge configuration has a larger “exposure” to any changes of the membrane and therefore the resulting energy recovery and power density become more sensitive to changes in the membrane properties.

References

- [1] V. G. Gude, "Desalination and water reuse to address global water scarcity," *Reviews in Environmental Science and Bio/Technology*, vol. 16, no. 4, pp. 591-609, 2017.
- [2] M. Elimelech and W. A. Phillip, "The future of seawater desalination: energy, technology, and the environment," *science*, vol. 333, no. 6043, pp. 712-717, 2011.
- [3] K. E. Rodman *et al.*, "Coastal California Wastewater Effluent as a Resource for Seawater Desalination Brine Commingling," *Water*, vol. 10, no. 3, p. 322, 2018.

- [4] C. Klaysom, T. Y. Cath, T. Depuydt, and I. F. Vankelecom, "Forward and pressure retarded osmosis: potential solutions for global challenges in energy and water supply," *Chemical society reviews*, vol. 42, no. 16, pp. 6959-6989, 2013.
- [5] T. Y. Cath, A. E. Childress, and M. Elimelech, "Forward osmosis: principles, applications, and recent developments," *Journal of membrane science*, vol. 281, no. 1-2, pp. 70-87, 2006.
- [6] F. Zaviska, Y. Chun, M. Heran, and L. Zou, "Using FO as pre-treatment of RO for high scaling potential brackish water: energy and performance optimisation," *Journal of membrane science*, vol. 492, pp. 430-438, 2015.
- [7] T. Y. Cath, J. E. Drewes, C. D. Lundin, and N. T. Hancock, "Forward osmosis—reverse osmosis process offers a novel hybrid solution for water purification and reuse," *IDA Journal of Desalination and Water Reuse*, vol. 2, no. 4, pp. 16-20, 2010.
- [8] N. T. Hancock, P. Xu, M. J. Roby, J. D. Gomez, and T. Y. Cath, "Towards direct potable reuse with forward osmosis: Technical assessment of long-term process performance at the pilot scale," *Journal of Membrane Science*, vol. 445, pp. 34-46, 2013. *Journal of Membrane Science*.
- [9] T. Y. Cath, N. T. Hancock, C. D. Lundin, C. Hoppe-Jones, and J. E. Drewes, "A multi-barrier osmotic dilution process for simultaneous desalination and purification of impaired water," *Journal of Membrane Science*, vol. 362, no. 1-2, pp. 417-426, 2010.
- [10] J. E. Kim, S. Phuntsho, S. M. Ali, J. Y. Choi, and H. K. Shon, "Forward osmosis membrane modular configurations for osmotic dilution of seawater by forward osmosis and reverse osmosis hybrid system," *Water research*, vol. 128, pp. 183-192, 2018. *Water research*.
- [11] K. Lutchimiah, A. Verliefe, K. Roest, L. C. Rietveld, and E. R. Cornelissen, "Forward osmosis for application in wastewater treatment: a review," *Water research*, vol. 58, pp. 179-197, 2014.
- [12] A. Altaee, G. J. Millar, G. Zaragoza, and A. Sharif, "Energy efficiency of RO and FO–RO system for high-salinity seawater treatment," *Clean technologies and Environmental policy*, vol. 19, no. 1, pp. 77-91, 2017.
- [13] G. Blandin, A. R. Verliefe, C. Y. Tang, and P. Le-Clech, "Opportunities to reach economic sustainability in forward osmosis–reverse osmosis hybrids for seawater desalination," *Desalination*, vol. 363, pp. 26-36, 2015.
- [14] F. Zaviska and L. Zou, "Using modelling approach to validate a bench scale forward osmosis pre-treatment process for desalination," *Desalination*, vol. 350, pp. 1-13, 2014.
- [15] R. V. Linares *et al.*, "Life cycle cost of a hybrid forward osmosis–low pressure reverse osmosis system for seawater desalination and wastewater recovery," *Water research*, vol. 88, pp. 225-234, 2016.
- [16] S. Benavides and W. A. Phillip, "Water recovery and solute rejection in forward osmosis modules: Modeling and bench-scale experiments," *Journal of membrane science*, vol. 505, pp. 26-35, 2016.
- [17] D. Attarde, M. Jain, and S. K. Gupta, "Modeling of a forward osmosis and a pressure-retarded osmosis spiral wound module using the Spiegler-Kedem model and experimental validation," *Separation and Purification Technology*, vol. 164, pp. 182-197, 2016.

- [18] Y.-J. Choi, J.-S. Choi, H.-J. Oh, S. Lee, D. R. Yang, and J. H. Kim, "Toward a combined system of forward osmosis and reverse osmosis for seawater desalination," *Desalination*, vol. 247, no. 1-3, pp. 239-246, 2009.
- [19] J. Jeon, J. Jung, S. Lee, J. Y. Choi, and S. Kim, "A simple modeling approach for a forward osmosis system with a spiral wound module," *Desalination*, vol. 433, pp. 120-131, 2018.
- [20] S. Phuntsho, S. Hong, M. Elimelech, and H. K. Shon, "Osmotic equilibrium in the forward osmosis process: Modelling, experiments and implications for process performance," *Journal of membrane science*, vol. 453, pp. 240-252, 2014.
- [21] B. Gu, D. Kim, J. Kim, and D. R. Yang, "Mathematical model of flat sheet membrane modules for FO process: Plate-and-frame module and spiral-wound module," *Journal of membrane science*, vol. 379, no. 1-2, pp. 403-415, 2011.
- [22] Y. C. Kim and S.-J. Park, "Experimental study of a 4040 spiral-wound forward-osmosis membrane module," *Environmental science & technology*, vol. 45, no. 18, pp. 7737-7745, 2011. *Environmental science & technology*.
- [23] J. Kim, G. Blandin, S. Phuntsho, A. Verliefde, P. Le-Clech, and H. Shon, "Practical considerations for operability of an 8 "spiral wound forward osmosis module: Hydrodynamics, fouling behaviour and cleaning strategy," *Desalination*, vol. 404, pp. 249-258, 2017.
- [24] M. Higa *et al.*, "Experimental study of a hollow fiber membrane module in pressure-retarded osmosis: Module performance comparison with volumetric-based power outputs," *Desalination*, vol. 420, pp. 45-53, 2017.
- [25] A. Achilli, J. L. Prante, N. T. Hancock, E. B. Maxwell, and A. E. Childress, "Experimental results from RO-PRO: a next generation system for low-energy desalination," *Environmental Science & Technology*, vol. 48, no. 11, pp. 6437-6443, 2014.
- [26] J. L. Prante, J. A. Ruskowitz, A. E. Childress, and A. Achilli, "RO-PRO desalination: an integrated low-energy approach to seawater desalination," *Applied Energy*, vol. 120, pp. 104-114, 2014.
- [27] R. L. Stover, "Seawater reverse osmosis with isobaric energy recovery devices," *Desalination*, vol. 203, no. 1-3, pp. 168-175, 2007.
- [28] C. Fritzmann, J. Löwenberg, T. Wintgens, and T. Melin, "State-of-the-art of reverse osmosis desalination," *Desalination*, vol. 216, no. 1-3, pp. 1-76, 2007.
- [29] J. W. Post *et al.*, "Salinity-gradient power: Evaluation of pressure-retarded osmosis and reverse electrodialysis," *Journal of membrane science*, vol. 288, no. 1-2, pp. 218-230, 2007.
- [30] Y. Tanaka *et al.*, "Experimental and simulation studies of two types of 5-inch scale hollow fiber membrane modules for pressure-retarded osmosis," *Desalination*, vol. 447, pp. 133-146, 2018.
- [31] Y. Chen *et al.*, "Module scale-up and performance evaluation of thin film composite hollow fiber membranes for pressure retarded osmosis," *Journal of Membrane Science*, vol. 548, pp. 398-407, 2018. *Journal of Membrane Science*.
- [32] J. Kim, M. Park, S. A. Snyder, and J. H. Kim, "Reverse osmosis (RO) and pressure retarded osmosis (PRO) hybrid processes: Model-based scenario study," *Desalination*, vol. 322, pp. 121-130, 2013. *Desalination*.

- [33] W. He, Y. Wang, A. Sharif, and M. H. Shaheed, "Thermodynamic analysis of a stand-alone reverse osmosis desalination system powered by pressure retarded osmosis," *Desalination*, vol. 352, pp. 27-37, 2014. *Desalination*.
- [34] A. Almansoori and Y. Saif, "Structural optimization of osmosis processes for water and power production in desalination applications," *Desalination*, vol. 344, pp. 12-27, 2014. *Desalination*.
- [35] S. Wang, Q. Zhu, C. He, B. Zhang, Q. Chen, and M. Pan, "Model-based optimization and comparative analysis of open-loop and closed-loop RO-PRO desalination systems," *Desalination*, vol. 446, pp. 83-93, 2018.
- [36] A. Achilli, T. Y. Cath, and A. E. Childress, "Power generation with pressure retarded osmosis: An experimental and theoretical investigation," *Journal of membrane science*, vol. 343, no. 1-2, pp. 42-52, 2009.
- [37] M. F. Naguib, J. Maisonneuve, C. B. Laflamme, and P. Pillay, "Modeling pressure-retarded osmotic power in commercial length membranes," *Renewable energy*, vol. 76, pp. 619-627, 2015. *Renewable energy*.
- [38] S. Lin, A. P. Straub, and M. Elimelech, "Thermodynamic limits of extractable energy by pressure retarded osmosis," *Energy & Environmental Science*, vol. 7, no. 8, pp. 2706-2714, 2014.
- [39] N. Y. Yip and M. Elimelech, "Thermodynamic and energy efficiency analysis of power generation from natural salinity gradients by pressure retarded osmosis," *Environmental science & technology*, vol. 46, no. 9, pp. 5230-5239, 2012. *Environmental science & technology*.
- [40] G. O'Toole, L. Jones, C. Coutinho, C. Hayes, M. Napoles, and A. Achilli, "River-to-sea pressure retarded osmosis: Resource utilization in a full-scale facility," *Desalination*, vol. 389, pp. 39-51, 2016.
- [41] G. Z. Ramon, B. J. Feinberg, and E. M. Hoek, "Membrane-based production of salinity-gradient power," *Energy & environmental science*, vol. 4, no. 11, pp. 4423-4434, 2011.
- [42] Y. Xu, X. Peng, C. Y. Tang, Q. S. Fu, and S. Nie, "Effect of draw solution concentration and operating conditions on forward osmosis and pressure retarded osmosis performance in a spiral wound module," *Journal of Membrane Science*, vol. 348, no. 1-2, pp. 298-309, 2010. *Journal of Membrane Science*.
- [43] X. Wei, Z. M. Binger, A. Achilli, K. T. Sanders, and A. E. Childress, "A modeling framework to evaluate blending of seawater and treated wastewater streams for synergistic desalination and potable reuse," *Water Research*, p. 115282, 2019.
- [44] W. He, Y. Wang, and M. H. Shaheed, "Enhanced energy generation and membrane performance by two-stage pressure retarded osmosis (PRO)," *Desalination*, vol. 359, pp. 186-199, 2015.
- [45] H. T. Innovation, "FO Element Datasheet," ed, 2014.
- [46] J. R. McCutcheon and M. Elimelech, "Modeling water flux in forward osmosis: implications for improved membrane design," *AIChE journal*, vol. 53, no. 7, pp. 1736-1744, 2007. *AIChE journal*.
- [47] A. Tiraferri, N. Y. Yip, A. P. Straub, S. R.-V. Castrillon, and M. Elimelech, "A method for the simultaneous determination of transport and structural parameters of forward osmosis membranes," *Journal of membrane science*, vol. 444, pp. 523-538, 2013.

- [48] W. A. Phillip, J. S. Yong, and M. Elimelech, "Reverse draw solute permeation in forward osmosis: modeling and experiments," *Environmental science & technology*, vol. 44, no. 13, pp. 5170-5176, 2010. Environmental science & technology.
- [49] S. Loeb, L. Titelman, E. Korngold, and J. Freiman, "Effect of porous support fabric on osmosis through a Loeb-Sourirajan type asymmetric membrane," *Journal of Membrane Science*, vol. 129, no. 2, pp. 243-249, 1997.
- [50] N. Y. Yip *et al.*, "Thin-film composite pressure retarded osmosis membranes for sustainable power generation from salinity gradients," *Environmental science & technology*, vol. 45, no. 10, pp. 4360-4369, 2011. Environmental science & technology.